

---

# DyMoDreamer: World Modeling with Dynamic Modulation

---

Boxuan Zhang<sup>1</sup>, Runqing Wang<sup>1</sup>, Wei Xiao<sup>1</sup>, Weipu Zhang<sup>1</sup>,  
 Jian Sun<sup>1</sup>, Gao Huang<sup>2</sup>, Jie Chen<sup>1</sup>, Gang Wang<sup>1\*</sup>

<sup>1</sup>School of Automation, Beijing Institute of Technology

<sup>2</sup>Department of Automation, BNRist, Tsinghua University

## Abstract

A critical bottleneck in deep reinforcement learning (DRL) is sample inefficiency, as training high-performance agents often demands extensive environmental interactions. Model-based reinforcement learning (MBRL) mitigates this by building world models that simulate environmental dynamics and generate synthetic experience, improving sample efficiency. However, conventional world models process observations holistically, failing to decouple dynamic objects and temporal features from static backgrounds. This approach is computationally inefficient, especially for visual tasks where dynamic objects significantly influence rewards and decision-making performance. To address this, we introduce DyMoDreamer, a novel MBRL algorithm that incorporates a dynamic modulation mechanism to improve the extraction of dynamic features and enrich the temporal information. DyMoDreamer employs differential observations derived from a novel inter-frame differencing mask, explicitly encoding object-level motion cues and temporal dynamics. Dynamic modulation is modeled as stochastic categorical distributions and integrated into a recurrent state-space model (RSSM), enhancing the model’s focus on reward-relevant dynamics. Experiments demonstrate that DyMoDreamer sets a new state-of-the-art on the Atari 100k benchmark with a 156.6% mean human-normalized score, establishes a new record of 832 on the DeepMind Visual Control Suite, and gains a 9.5% performance improvement after 1M steps on the Crafter benchmark. Our code is released at <https://github.com/Ultraman-Tiga1/DyMoDreamer>.

## 1 Introduction

Deep reinforcement learning (DRL) has achieved significant breakthroughs in sequential decision-making tasks [1, 2, 3, 4]. State-of-the-art methods such as DQN [5], PPO [6], MuZero [7], and EfficientZero [8] have demonstrated impressive performance across various benchmarks. However, these methods often suffer from low sample efficiency, requiring hundreds of millions of interactions with the environment [9], thus limiting their practicality for real-world applications where data collection is costly or infeasible. A key approach to addressing this challenge is the general framework of world models, which learns compact latent dynamics for planning and decision-making. One early instantiation of this framework [10], combines a VAE with an RNN and uses evolutionary strategies to optimize policies in the learned latent space. This framework combines a VAE with a recurrent neural network (RNN) and uses evolutionary strategies to optimize the policy within a latent space. By generating synthetic interaction data or “imagination trajectories” [11, 12], world models allow agents to learn behaviors entirely within the learned model. This model-based approach reduces the reliance on direct environment interactions, significantly improving sample efficiency.

---

\*Corresponding author: [gangwang@bit.edu.cn](mailto:gangwang@bit.edu.cn).

Traditionally, RNNs have been employed to capture temporal dependencies in world models. For instance, the Dreamer series (DreamerV1-3) [11, 13, 14] has demonstrated human-level performance on challenging benchmarks like Atari 100k [15] and Minecraft [16] using the recurrent state space model (RSSM) [17]. More recently, transformer-based world model architectures [18] have revolutionized sequence modeling, introducing methods such as GPT-like models [19] and Transformer-XL [20], and spatio-temporal transformers [21]. These advances have further refined the capabilities of world models through tokenization techniques [9, 22, 23].

Despite their success, both RSSM- and transformer-based world model architectures face challenges in accurately modeling small dynamic objects [24]. VAEs tend to amplify randomness, disproportionately affecting the parameters of temporal models [25]. Moreover, small dynamic objects often carry a higher degree of decision relevance compared to static environment backgrounds [26]. For example, in Atari’s game *Pong*, the paddle and ball are critical for decision-making, while the static red background is irrelevant. Recent techniques such as IRIS [9, 22, 23] and DIAMOND [24] partially mitigate these issues by improving the precision of image reconstruction in world modeling, but at the cost of significant computational overhead. Similarly, the recent approach OC-STORM [21] integrates vision models with world models, and introduces segmentation masks for object annotation, which require extensive pretraining and prior knowledge of object counts.

In this paper, we introduce DyMoDreamer, a novel world model architecture for model-based RL that improves dynamic feature extraction and enriches temporal information by encoding differential observations. DyMoDreamer integrates a dynamic modulation mechanism into RSSM, emphasizing critical environmental variations without relying on high-precision image reconstructions or prior object annotations. Through a novel lightweight inter-frame differencing mask, our approach effectively prioritizes decision-relevant dynamic features, addressing key limitations of existing RNN- and transformer-based models. Our approach is inspired by the cognitive processes observed in human infants, who naturally focus on dynamic object interactions to infer fundamental principles about their surroundings [27, 28]. Leveraging this principle, DyMoDreamer achieves superior policy performance, demonstrating that emphasizing dynamic objects and temporal information significantly improves decision-making in RL. Our method establishes a new SOTA with 156.6% human-normalized score on the Atari 100K benchmark, sets a new record with 832 mean score on the DeepMind Visual Control Suite, and delivers a 9.5% performance improvement on the Crafter benchmark after 1M environment steps.

Our main contributions are summarized as follows:

- We introduce a dynamic modulation mechanism that enhances RSSM by encoding differential observations to focus on key dynamic features and temporal information.
- We develop DyMoDreamer, a novel world model that integrates dynamic modulation into recurrent states, improving policy efficiency by prioritizing dynamic environmental features.
- We achieve state-of-the-art performance with 156.6% human-normalized score on the Atari 100k benchmark, 832 average score on DeepMind Visual Control, and 9.5% performance improvement on the Crafter benchmark within 1M steps.

The remainder of this paper is structured as follows. Section 2 details our methodology. Section 3 presents empirical evaluations on the Atari 100k benchmark, the DeepMind Visual Control Suite, and the Crafter benchmark, followed by ablation studies in Section 4. Detailed scores and curves are provided in Appendix E, alongside extensive ablation studies in Appendix K. We conclude with insights and future directions in Section 6.

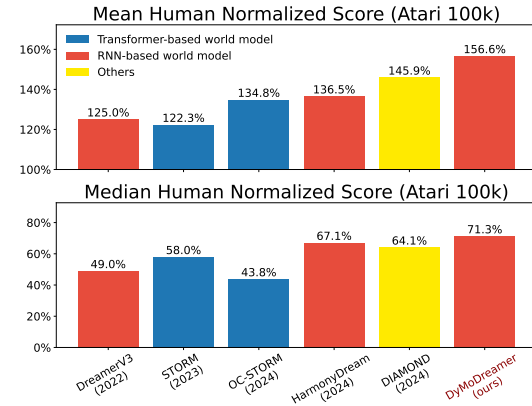


Figure 1: DyMoDreamer surpasses existing state-of-the-art model-based methods.

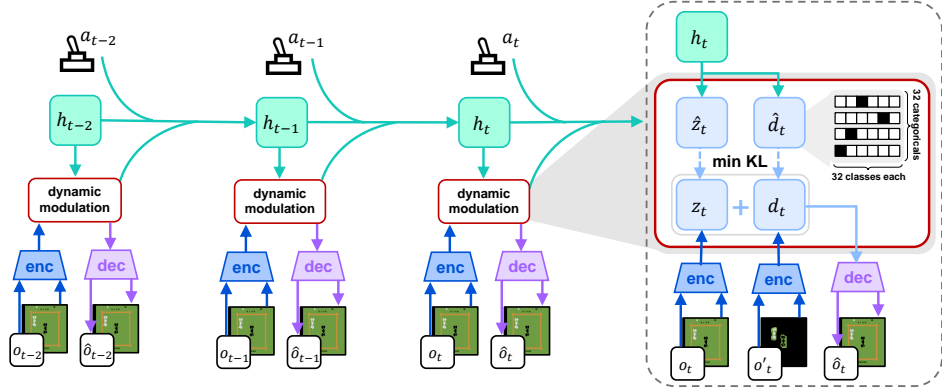


Figure 2: Overview of DyMoDreamer. The model integrates dynamic modulation derived from differential observations to enhance the perception of dynamic features within the environment.

## 2 Methodology

This section outlines DyMoDreamer, a model-based reinforcement learning algorithm designed to enhance dynamic feature extraction for improved agent performance. The problem is formulated as a partially observable Markov decision process (POMDP), represented by the tuple  $(\mathcal{O}, \mathcal{A}, \mathcal{T}, R, \gamma)$ , where  $o_t \in \mathcal{O}$  denotes high-dimensional image observations,  $a_t \in \mathcal{A}$  represents discrete actions generated by some policy  $\pi(a_t | o_{1:t}, a_{1:t-1})$ ,  $\mathcal{T}$  is the transition function,  $R$  is the reward function associated with a particular task, and  $\gamma$  is the discounting factor. The objective is to learn a policy  $\pi$  that maximizes the expected sum of discounted rewards  $\mathbb{E}_\pi [\sum_{t=1}^{\infty} \gamma^{t-1} r_t]$ , where  $r_t = R(o_{t-1}, a_{t-1})$ .

We present DyMoDreamer, a model-based RL framework designed to improve world model representations of dynamic temporal features and enhance agent performance. At its core, DyMoDreamer employs the RSSM architecture, augmented with novel dynamic modulation mechanisms that selectively emphasize dynamic features and temporal information in the environment. This approach draws inspiration from advances in modulated ordinary differential equations (ODEs) [29], where independently trained modulators improve temporal modeling for long-term prediction in complex systems. Moreover, the latent flow method [30] in model free reinforcement learning (MFRL) suggests that capturing temporal changes via time-based differencing can enhance transition modeling and improve the performance [31]. Building on these insights, DyMoDreamer introduces a temporal frame differencing method to refine the expressiveness of dynamic modulators, enabling the agent to leverage richer and more decision-relevant information for improved policy learning and performance.

We mainly base our approach on DreamerV3 [14], introducing dynamic modulation into the RSSM world model architecture. Below, we detail the construction of inter-frame differencing masks for dynamic modulation (Section 2.1), the integration of dynamic modulation into the world model (Section 2.2), and the end-to-end training process (Section 2.4).

### 2.1 Dynamic Modulation

As a core component of the world model, we leverage a VAE with convolutional neural networks (CNNs) to encode observations into stochastic state representations. The original encoder in DreamerV3 integrates temporal information, modeled by the hidden states  $h_t$  (introduced in Section 2.2 along with RSSM), and maps observations  $o_t$  to stochastic representations  $z_t$ . To focus on the dynamic aspects of the environment, we introduce dynamic modulation, which explicitly captures temporal changes between frames.

Differential observations  $o'_t$  are derived by computing inter-frame differences from the original observations, effectively isolating dynamic components. A dedicated dynamic encoder processes  $o'_t$  to generate dynamic modulators  $d_t$ , which participate in the reconstruction of  $o_t$  to ensure the

accurate extraction of dynamic features. The encoding process is as follows:

$$\begin{aligned} \text{Stochastic encoder: } & z_t \sim q_\phi(z_t | h_t, o_t) \\ \text{Dynamic encoder: } & d_t \sim q_\phi(d_t | h_t, o'_t) \\ \text{Decoder: } & \hat{o}_t = p_\phi(\hat{o}_t | h_t, z_t, d_t). \end{aligned} \quad (1)$$

The primary claim of this work is that explicitly integrating dynamic modulators, which capture dynamic environmental features, significantly enhances agent performance. By modeling features through differential signals, the approach improves the extraction of critical dynamic patterns and bolsters overall robustness [32]. To ensure the dynamic modulators emphasize decision-relevant patterns in the environment, we construct differential observations  $o'_t$  using a frame differencing method. Since forward differencing requires access to future information, we instead define a temporal backward differential binary function:

$$D(o_{i,h,w,c}, o_{i-k,h,w,c}) = \begin{cases} 1, & \text{if } \|o_{i,h,w,c} - o_{i-k,h,w,c}\|_2 > \epsilon \\ 0, & \text{others} \end{cases} \quad (2)$$

where  $\epsilon$  is a binary threshold value, set to 0.001 and  $k$  is an integer hyperparameter represents the differenced frames' interval (empirically set to 1, increasing  $k$  helps suppress potential static background flash),  $i$  is the time dimension,  $h$  and  $w$  are the spatial dimensions, and  $c$  is the channel dimension. In fact, very few pixels may exceed the threshold  $\epsilon$  after processing by  $D(\cdot)$ . To address this sparsity, we expand the regions of interest by filling the 0-pixel regions surrounding 1-pixel regions with 1's, a process achieved using convolution operations. This yields dynamic differential masks  $M(o_t)$ , which emphasize both the differing pixels between frames and their surrounding regions. Subsequently, the differential observations are defined as the masked original observations  $o'_t = M(o_t) \cdot o_t$  and are utilized to determine the dynamic modulators. This design explicitly extracts dynamic features from the observations, effectively capturing temporal changes rather than merely amplifying the influence of the most recent frame in the recurrent information. Unlike approaches that rely on sophisticated vision techniques, computing differential observations imposes negligible computational overhead while yielding notable performance gains (Section 3.2). Section 2.3 discusses the motivation for performing differencing in the observation space rather than in the latent space. Furthermore, additional results in Appendix G demonstrate that DyMoDreamer can flexibly adapt to different differencing strategies tailored to varying task environments. Differential observations across different benchmarks are provided in Appendix F.

## 2.2 Dynamically Modulated World Model

During interaction with the environment, DyMoDreamer collects observations, actions, and rewards into an experience dataset. After a predefined number of interactions, trajectories are sampled from this dataset to train both the world model and the categorical VAEs [33, 34]. The world model is built on RSSM, where the sequence model utilizes the recurrent latent state  $h_t$ , to predict the sequence of stochastic representations and dynamic modulators based on past actions  $a_{t-1}$ . The model state is formed by concatenating  $h_t$ ,  $z_t$  and  $d_t$ , enabling the prediction of rewards  $\hat{r}_t$  and episode continuation flags  $\hat{c}_t \in \{0, 1\}$ :

$$\begin{aligned} \text{Sequence model: } & h_t = f_\phi(h_{t-1}, z_{t-1}, d_{t-1}, a_{t-1}) \\ \text{Latent predictor: } & \hat{z}_t = p_\phi(\hat{z}_t | h_t) \\ \text{Dynamics predictor: } & \hat{d}_t = p_\phi(\hat{d}_t | h_t) \\ \text{Reward predictor: } & \hat{r}_t = p_\phi(\hat{r}_t | h_t, z_t, d_t) \\ \text{Continue predictor: } & \hat{c}_t = p_\phi(\hat{c}_t | h_t, z_t, d_t). \end{aligned} \quad (3)$$

Since directly modeling the dynamics from raw images is computationally expensive and prone to errors, we convert the observation  $o_t$  into latent stochastic categorical distributions  $q_\phi(z_t | h_t, o_t) = \mathcal{Z}_t$  for the latent variable  $z_t$ , which consists of 32 categories, each with 32 classes. Similarly, the dynamic modulator  $d_t$  is sampled from  $\mathcal{D}_t = q_\phi(d_t | h_t, o_t)$ , where  $\mathcal{D}_t$  also consists of 32 categories, each with 32 classes:

$$z_t \sim q_\phi(z_t | h_t, o_t) = \mathcal{Z}_t, \quad d_t \sim q_\phi(d_t | h_t, o'_t) = \mathcal{D}_t. \quad (4)$$

We apply the straight-through gradients trick [35] to maintain the gradients of representations and modulators, as sampling from a distribution inherently lacks gradients for backpropagation. The sequence model  $f_\phi$  takes as input the hidden state  $h_{t-1}$ , the stochastic representation  $z_{t-1}$ , the dynamic modulator  $d_{t-1}$ , and the action  $a_{t-1}$  from the previous step. Using this input, it computes a deterministic hidden state  $h_t$  via a gated recurrent unit (GRU) [36]. Multi-layer perceptrons (MLPs) then utilize  $h_t$ ,  $z_t$  and  $d_t$  to predict the current reward  $\hat{r}_t$ , the continuation flag  $\hat{c}_t$ , the dynamic modulation distribution  $\mathcal{D}_t$ , and the stochastic distribution  $\mathcal{Z}_t$ , respectively.

By design, the dynamic modulator  $d_t$  is time-varying, capturing dynamic features that enhance the model’s focus on decision-related dynamic objects and their surroundings in  $o_t$ . As a result, our world model demonstrates the following advantageous properties:

- *Dynamic feature embedding*: The dynamic modulator embeds dynamic features into the prediction models, compelling the model to prioritize decision-critical dynamic objects.
- *Temporal information capturing*: The dynamic modulator  $d_t$ , predicted by the hidden state  $h_t$ , enables the world model to capture temporal information across time sequences.
- *End-to-end joint training*: The dynamic modulator integrates into the reconstruction process alongside the stochastic representations and hidden states, facilitating end-to-end joint training of all world model components without requiring separate modulator training.

### 2.3 Intuition Behind Dynamic Modulation

In policy learning, rewards are predominantly influenced by the dynamic parts of observations and their adjacent static parts. For example, in the *Boxing* environment, the rewards are determined by effective jabs delivered by the agent, which involve dynamic elements (fists and arms) and their immediate static context (the body of the agent and its opponent) in the observations. Therefore, explicitly extracting dynamic local features in temporal sequences enhances the world model’s ability to focus on decision-critical features, thereby improving policy performance. Moreover, since not all tasks rely exclusively on dynamic features for decision-making. For instance, in the *Gopher* environment, both dynamic elements (e.g., gophers and tunnels) and static objects (e.g., carrots to be protected) are critical for earning rewards. To address this, DyMoDreamer retains the original stochastic representations while augmenting them with dynamic modulators. We provide visualizations in Appendix H, which show that  $z_t$  is indeed influenced by the dynamic modulation, leading to increased attention of  $z_t$  to the static factors.

We choose to perform differencing in the observation space rather than in the latent space (as done in prior MFRL work [30], by adding  $\delta_t = z_t - z_{t-1}$  to the sequence model), because the limited precision of latent encoding may hinder the detection of fine-grained dynamic features. For example, if a small but important object (such as the 1-pixel ball in *Pong*) is not captured in either  $z_t$  or  $z_{t-1}$ , the latent difference would fail to reflect this motion. In contrast, frame-level differencing can make such movements explicit in the pixel space, and the dynamic modulation can incorporate this temporal information into modulation, enriching the dynamics modeling. Our ablation in Appendix K.3 further supports this motivation.

### 2.4 End-to-end Learning

In general, the parameters of the world model, denoted as  $\phi$ , are optimized end-to-end to minimize three types of losses: the prediction loss  $\mathcal{L}_{\text{pred}}$ , the dynamics loss  $\mathcal{L}_{\text{dyn}}$ , and the representation loss  $\mathcal{L}_{\text{rep}}$ . This optimization is performed in a self-supervised manner using a batch of sequences comprising observations  $o_{1:T}$ , actions  $a_{1:T}$ , rewards  $r_{1:T}$ , and continuation flags  $c_{1:T}$ . To further enhance the model’s prediction performance, we introduce a differential divergence regularization term  $\mathcal{L}_{\text{reg}}$ , which leverages differential observations  $o'_{1:T}$  to capture the dynamical differences between consecutive frames. The total loss function is defined in Equation (5), where  $\omega_{\text{dyn}} = 0.5$  and  $\omega_{\text{rep}} = 0.1$  represent the weight coefficients for the respective loss terms:

$$\mathcal{L}(\phi) = \mathbb{E}_\phi \left[ \sum_{t=1}^T (\mathcal{L}_{\text{pred}}(\phi) + \omega_{\text{dyn}} \mathcal{L}_{\text{dyn}}(\phi) + \omega_{\text{rep}} \mathcal{L}_{\text{rep}}(\phi)) \right] + \mathcal{L}_{\text{reg}}(\phi). \quad (5)$$

The prediction loss  $\mathcal{L}_{\text{pred}}$  trains the categorical VAE to encode stochastic representations  $z_t$  and dynamic modulators  $d_t$  while reconstructing the input visual observations  $o_t$ . Additionally, it enables

the model to predict environment rewards and episode continuation flags, which are crucial for computing imagined trajectory returns during the behavior learning phase. The prediction loss comprises three components, as defined in Equation (6):

$$\mathcal{L}_{\text{pred}}(\phi) = \mathcal{L}_{\text{rec}}(\phi) + \mathcal{L}_{\text{rew}}(\phi) + \mathcal{L}_{\text{con}}(\phi) \quad (6)$$

where  $\mathcal{L}_{\text{rec}}(\phi) = -\ln p_{\phi}(o_t|h_t, z_t, d_t)$  denotes the reconstruction loss of the input image,  $\mathcal{L}_{\text{rew}}(\phi) = -\ln p_{\phi}(r_t|h_t, z_t, d_t)$  refers to the reward prediction loss, using a symlog two-hot loss, transforming the regression problem into a classification problem with soft targets, and  $\mathcal{L}_{\text{con}}(\phi) = -\ln p_{\phi}(c_t|h_t, z_t, d_t)$  corresponds to the continuation flag prediction loss, which is implemented as a cross-entropy loss.

The dynamics loss  $\mathcal{L}_{\text{dyn}}$  trains the sequence model to predict stochastic representations and dynamic modulators by minimizing the Kullback-Leibler (KL) divergence between the predicted and true distributions:

$$\begin{aligned} \mathcal{L}_{\text{dyn}}(\phi) = & \max(1, \text{KL}[\text{sg}(q_{\phi}(z_t | h_t, o_t)) \| p_{\phi}(\hat{z}_t | h_t)]) \\ & + \underbrace{\max(1, \text{KL}[\text{sg}(q_{\phi}(d_t | h_t, o'_t)) \| p_{\phi}(\hat{d}_t | h_t)])}_{\text{modulation's dynamic loss}}. \end{aligned} \quad (7)$$

Here,  $\text{sg}(\cdot)$  represents the stop-gradient operator, and the maximum operator clips the loss at 1 nat (approximately 1.44 bits) [37]. This “free-bit” operation prevents the loss terms from becoming excessively small, allowing the model to focus on other terms during training [38].

The representation loss  $\mathcal{L}_{\text{rep}}$  enforces consistency between the priors and posteriors of  $\mathcal{Z}_t$  and  $\mathcal{D}_t$ , allowing for a factorized dynamics predictor for efficient sampling during imagination training. It is defined as:

$$\begin{aligned} \mathcal{L}_{\text{rep}}(\phi) = & \max(1, \text{KL}[q_{\phi}(z_t | h_t, o_t) \| \text{sg}(p_{\phi}(\hat{z}_t | h_t))]) \\ & + \underbrace{\max(1, \text{KL}[q_{\phi}(d_t | h_t, o'_t) \| \text{sg}(p_{\phi}(\hat{d}_t | h_t))])}_{\text{modulation's representation loss}}. \end{aligned} \quad (8)$$

The differential divergence regularization  $\mathcal{L}_{\text{reg}}$  addresses the limitations of mean-squared error (MSE) loss, which primarily focuses on intra-frame differences. Instead,  $\mathcal{L}_{\text{reg}}$  forces the model to learn inter-frame variations, improving its awareness of dynamic changes [39]. Backward differences are computed as  $\Delta\hat{o}_t = \hat{o}_t - \hat{o}_{t-1}$  and  $\Delta o_t = o_t - o_{t-1}$ . These differences are transformed into probability distributions using the softmax function along the channel, height, and width dimensions:

$$\sigma(\Delta\hat{o}_t) = \frac{\exp(\Delta\hat{o}_t/\tau)}{\sum_{h,w,c} \exp(\Delta\hat{o}_t/\tau)}, \quad \sigma(\Delta o_t) = \frac{\exp(\Delta o_t/\tau)}{\sum_{h,w,c} \exp(\Delta o_t/\tau)}, \quad (9)$$

where  $\tau$  is a temperature parameter (empirically set to 0.1) to sharpen the distributions. The regularization term is then defined as the average KL divergence between these distributions across the batch  $B$ :

$$\mathcal{L}_{\text{reg}}(\phi) = \frac{1}{B} \sum \text{KL}(\sigma(\Delta\hat{o}) \| \sigma(\Delta o)). \quad (10)$$

## 2.5 Policy Learning

The policy in DyMoDreamer is trained exclusively on abstract trajectories predicted by the model using a standard actor-critic framework [40]. In our approach, the actor and critic operate on the concentration states  $s_t = \{h_t, z_t, d_t\}$ , leveraging the Markovian representations learned by the recurrent world model with dynamic modulation. Notably, due to the adoption of backward differential observations to encode the dynamic modulation, a random action is sampled for the initial frame to derive a single observation (or  $k$  frames when  $k > 1$ ) for starting the backward difference, resulting in  $o'_1$ . As we show in Figure 3, although the reconstruction loss of imagined trajectories shows no significant reduction, we observe that DyMoDreamer generates substantially less hallucination on dynamic patterns during imagination compared to DreamerV3, which fundamentally explains the performance gains brought by our dynamic modulation mechanism. The remaining setup closely follows DreamerV3 and is detailed in Appendix D.

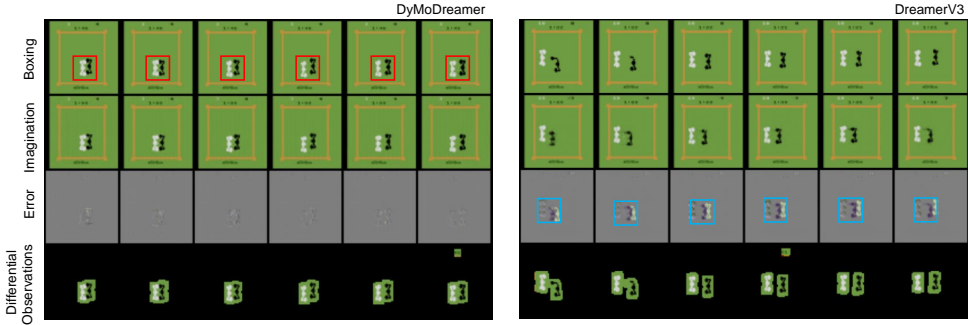


Figure 3: DyMoDreamer highlights the dynamic features. The players enclosed in red rectangles represent reward-relevant objects, which can be encoded into the dynamic modulation to enhance the RSSM. Blue rectangles mark the error regions where DreamerV3 exhibits hallucinations during the imagination reconstruction.

### 3 Experiments

#### 3.1 Benchmarks and Results

We evaluate DyMoDreamer on several widely-used benchmarks for sample-efficient RL: Atari 100k, DeepMind Visual Control Suite and Crafter. Table 1 summarizes the aggregate scores of DyMoDreamer and baselines, with the associated performance detailed per-environment scores and curves provided in Appendix E.

**Atari 100k Benchmark** We first evaluate DyMoDreamer on the Atari 100k benchmark, comprising 26 games from the Arcade Learning Environment, a widely adopted testbed for RL agents [15]. Agents are restricted to 100k actions (equivalent to 400k frames or  $\sim 1.85$  hours of gameplay) for training before evaluation. This constraint emphasizes sample efficiency, a critical metric in reinforcement learning. DyMoDreamer significantly improves upon the base method’s performance, and sets a new state-of-the-art benchmark with a mean human-normalized score (HNS) of 156.6%.

**DeepMind Visual Control Suite** To validate DyMoDreamer’s capacity for continuous control, we conduct experiments on the full set of 20 tasks in the DeepMind Visual Control Suite, challenging environments requiring policy learning from high-dimensional visual observations under a 1M step budget. In this suite, DyMoDreamer outperforms the newest and strongest existing baseline TWISTER [41], achieving a 5.5% average performance improvement over the DreamerV3 baseline. The results indicate that the dynamic modulation can also yield performance gains for world models in tasks involving high-dimensional observations and continuous action spaces.

**Crafter Benchmark** We finally complete the empirical validation using the Crafter [42] benchmark, which is a procedurally generated environment, inspired by the video game Minecraft, with visual inputs, a discrete action space and non-deterministic dynamics. In this benchmark, the background moves along with the agent, causing differential observations to capture the relative motion between the agent and the environmental components. Consequently, dynamic modulation enriches the information available for decision-making. On this benchmark, DyMoDreamer outperforms the IRIS series (the strongest transformer-based baselines) and achieves a 9.5% performance gain over the DreamerV3 baseline.

#### 3.2 Analysis and Implementation Details

We compared DyMoDreamer with methods leverage advanced architectures such as transformers and RSSMs, as well as diffusion models. Model-free and search-based approaches (e.g., BBF [43], EfficientZero [8]) are excluded, as our focus is the refinement of world models. Hyperparameters for DyMoDreamer follow DreamerV3 [14], except where explicitly noted, such as in the ablation studies.

Table 1: Aggregate scores of DyMoDreamer and baselines.

Atari 100k				
	OC-STORM (2025)	DIAMOND (2024)	DreamerV3 (2023)	DyMoDreamer (ours)
HNS Mean	134.8%	146%	125%	<b>156.6%</b>
HNS Median	43.8%	37%	49%	<b>71.3%</b>
DeepMind Visual Control Suite				
	TD-MPC2 (2023)	TWISTER (2025)	DreamerV3 (2023)	DyMoDreamer (ours)
Task Mean	720.9	801.8	786	<b>832</b>
Task Median	795.9	<b>907.6</b>	861	871
Crafter				
	IRIS (2023)	$\Delta$ -IRIS (2024)	DreamerV3 (2023)	DyMoDreamer (ours)
Return @1M	5.5	7.7	9.4	<b>10.3</b>

DyMoDreamer demonstrates superior performance compared to previous methods in environments where the key objects related to rewards are sparse and independent with each other, such as *Pong* and *Finger Spin*. This advantage can be attributed to the accurate capturing of dynamic modulators, which explicitly enhances the world model awareness of temporal features in the observations. DyMoDreamer also excels in tasks with distinct phases, such as *Krull*, and Crafter, as the predictable dynamic modulators explicitly guides the world model to capture transitions between task stages. Moreover, even when the reward signal is not fully captured by the dynamic information, DyMoDreamer still yields performance gains by explicitly retaining the stochastic representations, for example, *Gopher*. It's noteworthy that this enhancement is achieved without leveraging any additional techniques from the computer vision domain, thereby incurring no extra oversized computational overhead. By introducing dynamic modulation into the world model, we fully exploit the intrinsic potential of the RSSM framework, thereby enhancing the significance of our contribution. In our experiments, we use a machine with an NVIDIA 4090 graphics card with 8 CPU cores and 24 GB RAM. Training DyMoDreamer on one Atari game for 100k steps took roughly 5.5 hours in our JAX implementation.

## 4 Ablation Studies

Our experiments have shown incorporating dynamic modulators into the world model can greatly enhance the final outcomes. To further investigate this, we perform ablation studies on the two novel components introduced in DyMoDreamer: the dynamic modulation (Section 4.1) and the differential divergence regularization  $\mathcal{L}_{\text{reg}}$  (Section 4.2). We select four representative game environments: *Boxing*, featuring large and sparse dynamic objects; *Krull*, characterized by small and numerous dynamic objects; *Pong*, with small and sparse dynamic objects; and *Road Runner*, which includes both small and large dynamic objects.

### 4.1 Removing Dynamic Modulation

We first perform an ablation study where the dynamic modulators are retained while its integration into RSSM is removed, in order to assess the necessity of incorporating dynamic modulation for achieving performance gains. In this setting, the sequence model in Equation 3 degenerates to  $h_t = f_\phi(h_{t-1}, z_{t-1}, a_{t-1})$ , where the dynamic modulation is only involved in encoding and image reconstruction. Additionally, the constraints on the modulators  $d_t$  are removed from both  $\mathcal{L}_{\text{dyn}}$  and  $\mathcal{L}_{\text{dyn}}$ . As shown in Figure 4, removing the dynamic modulation mechanism causes a notable performance drop. Simply appending differential observations, without integrating them into the RSSM, fails to direct the world model's focus toward dynamic patterns. This result is comparable to the ablation in Appendix K.1, where increasing the dimensionality of  $z_t$  alone offers limited benefits. These findings indicate that the dynamic modulation should be embedded into the sequence model to

be effective. By integrating information from the predictable modulators into the recurrent state, the agent gains access to richer environment cues during decision-making, beyond merely increasing the dimensionality of the VAE.

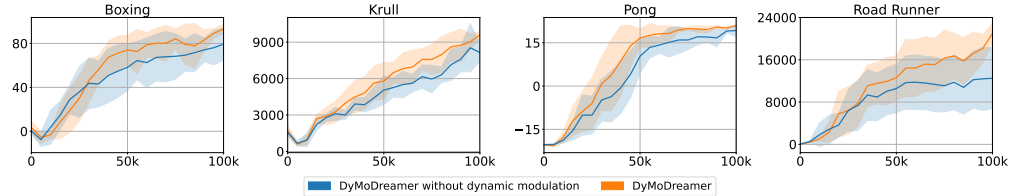


Figure 4: Ablation study on the dynamic modulation.

## 4.2 Differential Divergence Regularization

The differential divergence regularization  $\mathcal{L}_{\text{reg}}$  addresses the limitations of mean-squared error (MSE) loss, which primarily focuses on intra-frame differences. Therefore, we remove this component from DyMoDreamer and observe a performance drop (Figure 5), which demonstrates that the differential divergence regularization acts as a complementary supervisory signal that works in concert with reconstruction objectives, and contributes improvement through its unique ability to constrain the temporal consistency in the reconstruction process. Removing the differential divergence regularization leads to a performance drop; however, thanks to the dynamic modulation mechanism, the model still surpasses vanilla DreamerV3.

## 5 Related Work

World model-based reinforcement learning enables agents to learn via imagination, improving sample efficiency by predicting future states and rewards from compact latent representations. Early works like SimPLE [12] and Dreamer [11] pioneered latent dynamics modeling for decision-making. DreamerV2 [13] introduced discrete latents to mitigate compounding errors, and DreamerV3 [14] extended this to diverse domains with fixed hyperparameters. HarmonyDream [44] further refined training via adaptive loss balancing. Recent advances leverage transformers (e.g., STORM [25] and OC-STORM [21]) for scalable sequence modeling, with innovations like object-centric prediction. The IRIS series [9, 22] advanced tokenized imagination by employing VQ-VAE [45] to encode observations into discrete codes, compressing visual inputs into a compact symbolic space that facilitates long-horizon predictions. Meanwhile, DIAMOND [24] applies score-based diffusion models in pixel space for detailed visual modeling. Hierarchical world models (e.g., THICK [46], HIEROS [47], and Puppeteer [48]) further improve temporal abstraction, enabling long-horizon reasoning and coordination in complex environments.

## 6 Conclusion

In this work, we propose DyMoDreamer, a novel world modeling approach with dynamic modulation, which outperforms previous model-based methods in Atari 100k, DeepMind Visual Control and Crafter benchmarks, setting a new record for the RSSM architecture [17]. DyMoDreamer integrates dynamic modulation into RSSM, enabling the agent to effectively capture decision-relevant dynamic features and temporal information within the environment throughout the decision-making process. We capture dynamic features and temporal information by encoding differential observations, and enhance dynamic modulation with specialized dynamics and representation losses to improve its ability to integrate dynamic information. This design significantly improves the performance of the world model. Our work demonstrates that the RSSM framework remains highly promising and opens numerous avenues for future research. One potential direction is to introduce soft predictive constraints on future states during end-to-end training could prove beneficial [49, 50]. We believe that designing more human-like world model algorithms by learning from human’s cognitive behaviors holds significant potential for impact and represents an exciting path for exploration.

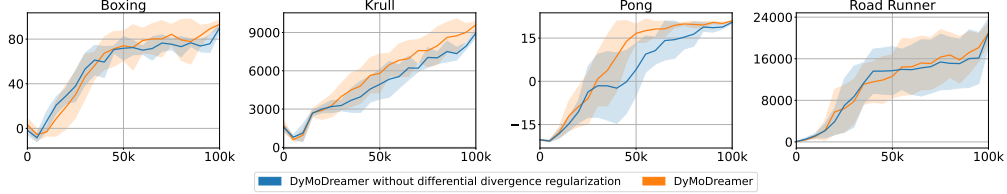


Figure 5: Ablation study on the differential divergence regularization.

## 7 Acknowledgments and Disclosure of Funding

We would like to thank all anonymous reviewers for their time, constructive comments, and engaging discussions. The work was supported by the National Natural Science Foundation of China under Grants U23B2059, 62173034, and 62495090.

## References

- [1] David Silver, Aja Huang, Chris J Maddison, Arthur Guez, Laurent Sifre, George Van Den Driessche, Julian Schrittwieser, Ioannis Antonoglou, Veda Panneershelvam, Marc Lanctot, et al. Mastering the game of Go with deep neural networks and tree search. *Nature*, 529(7587):484–489, 2016.
- [2] Jonas Degrave, Federico Felici, Jonas Buchli, Michael Neunert, Brendan Tracey, Francesco Carpanese, Timo Ewalds, Roland Hafner, Abbas Abdolmaleki, Diego de Las Casas, et al. Magnetic control of tokamak plasmas through deep reinforcement learning. *Nature*, 602(7897):414–419, 2022.
- [3] Nicklas Hansen, Hao Su, and Xiaolong Wang. TD-MPC2: Scalable, robust world models for continuous control. *arXiv preprint arXiv:2310.16828*, 2023.
- [4] Zhaohan Feng, Ruiqi Xue, Lei Yuan, Yang Yu, Ning Ding, Meiqin Liu, Bingzhao Gao, Jian Sun, Xinhua Zheng, and Gang Wang. Multi-agent embodied AI: Advances and future directions. *arXiv preprint arXiv:2505.05108*, 2025.
- [5] Volodymyr Mnih, Koray Kavukcuoglu, David Silver, Andrei A Rusu, Joel Veness, Marc G Bellemare, Alex Graves, Martin Riedmiller, Andreas K Fidjeland, Georg Ostrovski, et al. Human-level control through deep reinforcement learning. *nature*, 518(7540):529–533, 2015.
- [6] John Schulman, Filip Wolski, Prafulla Dhariwal, Alec Radford, and Oleg Klimov. Proximal policy optimization algorithms. *arXiv preprint arXiv:1707.06347*, 2017.
- [7] Julian Schrittwieser, Ioannis Antonoglou, Thomas Hubert, Karen Simonyan, Laurent Sifre, Simon Schmitt, Arthur Guez, Edward Lockhart, Demis Hassabis, Thore Graepel, et al. Mastering Atari, Go, Chess and Shogi by planning with a learned model. *Nature*, 588(7839):604–609, 2020.
- [8] Weirui Ye, Shaohuai Liu, Thanard Kurutach, Pieter Abbeel, and Yang Gao. Mastering Atari games with limited data. In *Advances in Neural Information Processing Systems*, 2021.
- [9] Vincent Micheli, Eloi Alonso, and François Fleuret. Transformers are sample-efficient world models. *arXiv preprint arXiv:2209.00588*, 2022.
- [10] David Ha and Jürgen Schmidhuber. World models. *arXiv preprint arXiv:1803.10122*, 2018.
- [11] Danijar Hafner, Timothy Lillicrap, Jimmy Ba, and Mohammad Norouzi. Dream to control: Learning behaviors by latent imagination. *arXiv preprint arXiv:1912.01603*, 2019.
- [12] Lukasz Kaiser, Mohammad Babaeizadeh, Piotr Milos, Blazej Osinski, Roy H Campbell, Konrad Czechowski, Dumitru Erhan, Chelsea Finn, Piotr Kozakowski, Sergey Levine, et al. Model-based reinforcement learning for Atari. *arXiv preprint arXiv:1903.00374*, 2019.

- [13] Danijar Hafner, Timothy Lillicrap, Mohammad Norouzi, and Jimmy Ba. Mastering Atari with discrete world models. *arXiv preprint arXiv:2010.02193*, 2020.
- [14] Danijar Hafner, Jurgis Pasukonis, Jimmy Ba, and Timothy Lillicrap. Mastering diverse domains through world models. *arXiv preprint arXiv:2301.04104*, 2023.
- [15] Marc G Bellemare, Yavar Naddaf, Joel Veness, and Michael Bowling. The arcade learning environment: An evaluation platform for general agents. *Journal of Artificial Intelligence Research*, 47:253–279, 2013.
- [16] Ingmar Kanitscheider, Joost Huizinga, David Farhi, William Hebgen Guss, Brandon Houghton, Raul Sampedro, Peter Zhokhov, Bowen Baker, Adrien Ecoffet, Jie Tang, et al. Multi-task curriculum learning in a complex, visual, hard-exploration domain: Minecraft. *arXiv preprint arXiv:2106.14876*, 2021.
- [17] Danijar Hafner, Timothy Lillicrap, Ian Fischer, Ruben Villegas, David Ha, Honglak Lee, and James Davidson. Learning latent dynamics for planning from pixels. In *International conference on machine learning*, pages 2555–2565. PMLR, 2019.
- [18] A Vaswani. Attention is all you need. In *Advances in Neural Information Processing Systems*, 2017.
- [19] Alec Radford. Improving language understanding by generative pre-training. 2018.
- [20] Zihang Dai, Zhilin Yang, Yiming Yang, Jaime Carbonell, Quoc V Le, and Ruslan Salakhutdinov. Transformer-XL: Attentive language models beyond a fixed-length context. *arXiv preprint arXiv:1901.02860*, 2019.
- [21] Weipu Zhang, Adam Jelley, Trevor McInroe, and Amos Storkey. Objects matter: Object-centric world models improve reinforcement learning in visually complex environments, 2025.
- [22] Vincent Micheli, Eloi Alonso, and François Fleuret. Efficient world models with context-aware tokenization. *arXiv preprint arXiv:2406.19320*, 2024.
- [23] Lior Cohen, Kaixin Wang, Bingyi Kang, and Shie Mannor. Improving token-based world models with parallel observation prediction. *arXiv preprint arXiv:2402.05643*, 2024.
- [24] Eloi Alonso, Adam Jelley, Vincent Micheli, Anssi Kanervisto, Amos Storkey, Tim Pearce, and François Fleuret. Diffusion for world modeling: Visual details matter in Atari. *arXiv preprint arXiv:2405.12399*, 2024.
- [25] Weipu Zhang, Gang Wang, Jian Sun, Yetian Yuan, and Gao Huang. STORM: Efficient stochastic transformer based world models for reinforcement learning. In *Advances in Neural Information Processing Systems*, 2023.
- [26] Quentin Delfosse, Jannis Blümli, Bjarne Gregori, Sebastian Sztwiertnia, and Kristian Kersting. OcAtari: Object-centric Atari 2600 reinforcement learning environments. *arXiv preprint arXiv:2306.08649*, 2023.
- [27] Elizabeth S Spelke. Principles of object perception. *Cognitive science*, 14(1):29–56, 1990.
- [28] Martha E Arterberry and Marc H Bornstein. Infant perceptual and conceptual categorization: The roles of static and dynamic stimulus attributes. *Cognition*, 86(1):1–24, 2002.
- [29] Ilze Amanda Auzina, Çağatay Yıldız, Sara Magliacane, Matthias Bethge, and Efstratios Gavves. Modulated neural ODEs. In *Advances in Neural Information Processing Systems*, 2024.
- [30] Wenling Shang, Xiaofei Wang, Aravind Srinivas, Aravind Rajeswaran, Yang Gao, Pieter Abbeel, and Michael Laskin. Reinforcement learning with latent flow. In *Advances in Neural Information Processing Systems*, 2021.
- [31] Yangru Huang, Peixi Peng, Yifan Zhao, Yunpeng Zhai, Haoran Xu, and Yonghong Tian. Simoun: Synergizing interactive motion-appearance understanding for vision-based reinforcement learning. In *International Conference on Computer Vision*. IEEE, 2023.

[32] Tianzhu Ye, Li Dong, Yuqing Xia, Yutao Sun, Yi Zhu, Gao Huang, and Furu Wei. Differential transformer. *arXiv preprint arXiv:2410.05258*, 2024.

[33] Diederik P Kingma. Auto-encoding variational Bayes. In *International Conference on Learning Representations*, 2014.

[34] Michał Kempka, Marek Wydmuch, Grzegorz Runc, Jakub Toczek, and Wojciech Jaśkowski. Vizdoom: A doom-based AI research platform for visual reinforcement learning. In *Conference on Computational Intelligence and Games*, pages 1–8, 2016.

[35] Yoshua Bengio, Nicholas Léonard, and Aaron Courville. Estimating or propagating gradients through stochastic neurons for conditional computation. *arXiv preprint arXiv:1308.3432*, 2013.

[36] Rahul Dey and Fathi M Salem. Gate-variants of gated recurrent unit (GRU) neural networks. In *International Midwest Symposium on Circuits and Systems*, pages 1597–1600. IEEE, 2017.

[37] Chang Chen, Yi-Fu Wu, Jaesik Yoon, and Sungjin Ahn. Transdreamer: Reinforcement learning with transformer world models. *arXiv preprint arXiv:2202.09481*, 2022.

[38] Durk P Kingma, Tim Salimans, Rafal Jozefowicz, Xi Chen, Ilya Sutskever, and Max Welling. Improved variational inference with inverse autoregressive flow. In *Advances in neural information processing systems*, volume 29, 2016.

[39] Cheng Tan, Zhangyang Gao, Lirong Wu, Yongjie Xu, Jun Xia, Siyuan Li, and Stan Z Li. Temporal attention unit: Towards efficient spatiotemporal predictive learning. In *Proceedings of the IEEE/CVF Conference on Computer Vision and Pattern Recognition*, pages 18770–18782, 2023.

[40] Richard S Sutton. Dyna, an integrated architecture for learning, planning, and reacting. *ACM Sigart Bulletin*, 2(4):160–163, 1991.

[41] Maxime Burchi and Radu Timofte. Learning Transformer-based world models with contrastive predictive coding. *arXiv preprint arXiv:2503.04416*, 2025.

[42] Danijar Hafner. Benchmarking the spectrum of agent capabilities. In *International Conference on Learning Representations*, 2022.

[43] Max Schwarzer, Johan Samir Obando Ceron, Aaron Courville, Marc G Bellemare, Rishabh Agarwal, and Pablo Samuel Castro. Bigger, better, faster: Human-level Atari with human-level efficiency. In *International Conference on Machine Learning*, pages 30365–30380. PMLR, 2023.

[44] Haoyu Ma, Jialong Wu, Ningya Feng, Chenjun Xiao, Dong Li, HAO Jianye, Jianmin Wang, and Mingsheng Long. HarmonyDream: Task harmonization inside world models. In *International Conference on Machine Learning*, 2024.

[45] Aaron Van Den Oord, Oriol Vinyals, et al. Neural discrete representation learning. In *Advances in Neural Information Processing Systems*, 2017.

[46] Christian Gumbsch, Noor Sajid, Georg Martius, and Martin V Butz. Learning hierarchical world models with adaptive temporal abstractions from discrete latent dynamics. In *International Conference on Learning Representations*, 2023.

[47] Paul Mattes, Rainer Schlosser, and Ralf Herbrich. Hieros: Hierarchical imagination on structured state space sequence world models. In *International Conference on Machine Learning*, 2024.

[48] Nicklas Hansen, Jyothir SV, Vlad Sobal, Yann LeCun, Xiaolong Wang, and Hao Su. Hierarchical world models as visual whole-body humanoid controllers. *arXiv preprint arXiv:2405.18418*, 2024.

[49] Max Schwarzer, Ankesh Anand, Rishab Goel, R Devon Hjelm, Aaron Courville, and Philip Bachman. Data-efficient reinforcement learning with self-predictive representations. *arXiv preprint arXiv:2007.05929*, 2020.

[50] Pierluca D’Oro, Max Schwarzer, Evgenii Nikishin, Pierre-Luc Bacon, Marc G Bellemare, and Aaron Courville. Sample-efficient reinforcement learning by breaking the replay ratio barrier. In *In Advances in Neural Information Processing Systems*, 2022.

[51] Matteo Hessel, Joseph Modayil, Hado Van Hasselt, Tom Schaul, Georg Ostrovski, Will Dabney, Dan Horgan, Bilal Piot, Mohammad Azar, and David Silver. Rainbow: Combining improvements in deep reinforcement learning. In *Proceedings of the AAAI Conference on Artificial Intelligence*, volume 32, 2018.

[52] Jan Robine, Marc Höftmann, Tobias Uelwer, and Stefan Harmeling. Transformer-based world models are happy with 100k interactions. *arXiv preprint arXiv:2303.07109*, 2023.

[53] Lior Cohen, Kaixin Wang, Bingyi Kang, and Shie Mannor. Improving token-based world models with parallel observation prediction. In *In International Conference on Machine Learning*, 2024.

[54] Ho Kei Cheng, Seoung Wug Oh, Brian Price, Joon-Young Lee, and Alexander Schwing. Putting the object back into video object segmentation. In *Proceedings of the IEEE/CVF Conference on Computer Vision and Pattern Recognition*, pages 3151–3161, 2024.

[55] Nolan Wagener, Andrey Kolobov, Felipe Vieira Frujeri, Ricky Loynd, Ching-An Cheng, and Matthew Hausknecht. MoCapAct: A multi-task dataset for simulated humanoid control. In *Advances in Neural Information Processing Systems*, 2022.

[56] Marc G Bellemare, Will Dabney, and Rémi Munos. A distributional perspective on reinforcement learning. In *International conference on machine learning*, pages 449–458, 2017.

[57] TP Lillicrap. Continuous control with deep reinforcement learning. *arXiv preprint arXiv:1509.02971*, 2015.

[58] Richard S Sutton and Andrew G Barto. *Reinforcement Learning: An Introduction*. MIT press, 2018.

[59] Sukjun Hwang, Miran Heo, Seoung Wug Oh, and Seon Joo Kim. Video instance segmentation using inter-frame communication transformers. In *Advances in Neural Information Processing Systems*, 2021.

[60] Tongzhou Wang, Simon S Du, Antonio Torralba, Phillip Isola, Amy Zhang, and Yuandong Tian. Denoised mdps: Learning world models better than the world itself. *arXiv preprint arXiv:2206.15477*, 2022.

[61] Ignat Georgiev, Varun Giridhar, Nicklas Hansen, and Animesh Garg. PWM: Policy learning with large world models. *arXiv preprint arXiv:2407.02466*, 2024.

[62] Tianhe Yu, Deirdre Quillen, Zhanpeng He, Ryan Julian, Karol Hausman, Chelsea Finn, and Sergey Levine. Meta-world: A benchmark and evaluation for multi-task and meta reinforcement learning. In *Conference on Robot Learning*, pages 1094–1100, 2020.

[63] Yuval Tassa, Yotam Doron, Alistair Muldal, Tom Erez, Yazhe Li, Diego de Las Casas, David Budden, Abbas Abdolmaleki, Josh Merel, Andrew Lefrancq, et al. Deepmind control suite. *arXiv preprint arXiv:1801.00690*, 2018.

[64] Alex Kendall, Yarin Gal, and Roberto Cipolla. Multi-task learning using uncertainty to weigh losses for scene geometry and semantics. In *Proceedings of the IEEE Conference on Computer Vision and Pattern Recognition*, pages 7482–7491, 2018.

## A Further Related Work

Model-based RL utilizing world models enables “learning through imagination” to provide greater data efficiency and offers a promising approach [12]. These algorithms use self-supervised manners to construct parameterized simulation world models of the environments, leveraging losses such as reconstructing observations with decoders, predicting rewards and states at the next step, and the

consistency between prior and posterior of latent states. Agent learns behaviors by the imagination trajectories based on world model predictions, reducing the reliance on environment interactions and improving the sample efficiency. SimPLe [12] applied world models to enable agents to focus on sample efficiency, and solve Atari games with fewer interactions than model-free Rainbow [51]. Dreamer [11] pioneered the reinforcement learning directly from the latent space of a recurrent state space model. Building on this, DreamerV2 [13] demonstrated that employing discrete latent variables mitigates compounding errors, while DreamerV3 [14] further advanced the approach, achieving human-level performance across diverse domains using fixed hyperparameters. HarmonyDream [44] employed a harmonious loss to dynamically adjust the weights of different loss terms during training. This approach ensures that the losses of various tasks, such as image reconstruction and reward modeling, remain within the same order of magnitude throughout the end-to-end training process.

Following the success of the Dreamer algorithm [11], the transformer architectures [18] are also rapidly adopted for its superior training efficiency and favorable scaling properties. TWM [52] utilized the Transformer-XL [20] architecture to learn long-term dependencies while staying computationally efficient. IRIS [9] and  $\Delta$ -IRIS [22] utilized VQ-VAE [45] to build a language of image tokens to represent observations and make decisions based on the reconstructed observations. Building upon the IRIS framework, REM introduced a novel parallel observation prediction mechanism to enhance the imagination, and achieves performance surpassing the baseline [53]. STORM [25] used GPT-like architecture with a different tokenization approach, which captures long-term dependencies through attention mechanism and achieves impressive performance on the Atari 100k benchmark. OC-STORM extracted object features through a parameter-frozen pre-trained foundation vision model “Cutie” [54] to apply both these object features and the raw observations as inputs for training an object-centric world model, which predicts the dynamic objects in the environment while considering the relationships between different objects and the background. Additionally, DIAMOND [24] introduced a diffusion-based world model that operates entirely within the image space, enabling more accurate modeling of critical visual details in the world model.

Another type of world model adopts a hierarchical structure, this architecture operates at different time scales, allowing the agent to learn and make decisions across multiple levels of abstraction. [46] deploys a hierarchy of world models with a look ahead trajectory search approach called THICK, which learns the world model via discrete latent dynamics. The lower level of THICK updates parts of its latent state sparsely over time, forming invariant contexts. The higher level exclusively predicts situations that involve context changes. HIEROS proposed an S5 layer-based world model, which learned time abstracted world representations and imagines trajectories at multiple time scales in latent space [47]. Puppeteer [48] proposed hierarchical world model in which a high-level agent generates commands based on visual observations for a low-level agent to execute, and produces highly performant control policies in 8 tasks with a simulated 56-DoF humanoid [55], while synthesizing motions that are broadly preferred by humans.

## B Limitations

DyMoDreamer improves the temporal world modeling through dynamic modulation, yet fundamental limitations of MBRL remain. Accurately capturing environment dynamics, especially in visually complex or highly uncertain environments continues to be a key challenge. Compounding errors during long-horizon imagination hinder policy performance, and recurrent latent models offer limited capacity for long-term memory. Although DyMoDreamer partially addresses these issues via architectural enhancements, future work may benefit from integrating memory-augmented transformers or hierarchical abstractions to improve long-term reasoning. Moreover, despite gains in sample efficiency, the trade-off between model fidelity and policy stability persists. Generalization to real-world domains and robustness under distributional shifts remain critical open problems.

## C Broader Impacts

Training agents for real-world applications, such as robotics and autonomous driving, is challenging due to high costs, safety risk, and potential harm to humans. To mitigate these concerns, we conduct all experiments in simulated environments, eliminating risks associated with real-world training. We introduce DyMoDreamer, a world model with dynamic modulation that enables agents to learn through imagination rather than direct physical interactions. By reducing reliance on real-world data

collection, our approach enhances the safety and feasibility of deploying model-based reinforcement learning in safety-critical domains. This work contributes to the development of efficient and ethically responsible autonomous systems, addressing key concerns in real-world AI deployment.

## D Policy Learning

The policy learning approach closely follows that of DreamerV3 [14], with modifications specific to our method. To our DyMoDreamer, the actor and critic operate on the concentration states  $s_t = \{z_t, h_t, d_t\}$ . We select actions by sampling from the actor network and aim to maximize the return  $R_t = \sum_{\tau=1}^{\infty} \gamma^\tau r_{t+\tau}$  with a discount factor  $\gamma = 0.997$  for each state. The critic learns [56] to approximate the distribution of returns for each state under the current actor behavior:

$$\begin{aligned} \text{Actor: } a_t &\sim \pi_\theta(a_t | s_t) \\ \text{Critic: } V_\psi(R_t | s_t) &\approx \mathbb{E}_{\pi_\theta, p_\phi} \left[ \sum_{\tau=0}^{\infty} \gamma^\tau r_{t+\tau} \right], \end{aligned} \quad (11)$$

where the predicted values from the critic is a expectation of the distribution it predicts. We adopt the actor and critic learning settings from DreamerV3. The complete loss of the actor-critic algorithm is described by Equation (7), where  $\hat{r}_t$  corresponds to the reward predicted by the world model, and  $\hat{c}_t$  represents the predicted continuation flag. The critic learns to approximate the distribution of the return estimates  $R_t^\lambda$  using the maximum likelihood loss:

$$\mathcal{L}(\psi) = \frac{1}{BL} \sum_{n=1}^B \sum_{t=1}^L \left[ (V_\psi(s_t) - \text{sg}(R_t^\lambda))^2 + (V_\psi(s_t) - \text{sg}(V_{\psi^{\text{EMA}}}(s_t)))^2 \right], \quad (12)$$

where the constant  $L$  represent the imagination horizon and  $V_{\psi^{\text{EMA}}}$  is the exponential moving average (EMA) of the critic network  $\psi$  for stabilizing training and preventing overfitting [57].

For the actor network, we use the Reinforce estimator for both discrete and continuous actions, resulting in the surrogate loss function:

$$\mathcal{L}(\theta) = \frac{1}{BL} \sum_{n=1}^B \sum_{t=1}^L \left[ -\text{sg} \left( \frac{R_t^\lambda - V_\psi(s_t)}{\max(1, S)} \right) \ln \pi_\theta(a_t | s_t) - \eta H(\pi_\theta(a_t | s_t)) \right], \quad (13)$$

where  $H(\cdot)$  denotes the entropy of the policy distribution, while constants  $\eta$  represent the coefficient for entropy loss. The  $\lambda$ -return  $R_t^\lambda$  [58] is recursively defined as follows

$$\begin{aligned} R_t^\lambda &= r_t + \lambda c_t \left[ (1 - \lambda) V_\psi(s_{t+1}) + \lambda R_{t+1}^\lambda \right], \\ R_L^\lambda &= V_\psi(s_L). \end{aligned} \quad (14)$$

The normalization ratio  $S$  utilized in the actor loss (14) is defined in (15), which is computed as the range between the 5<sup>th</sup> and 95<sup>th</sup> percentiles of the  $\lambda$ -return  $R_t^\lambda$  across the batch:

$$S = \text{percentile}(R_t^\lambda, 95) - \text{percentile}(R_t^\lambda, 5). \quad (15)$$

## E Experimental Details

### E.1 Atari 100k Experiments

We evaluate agent performance over 100 episodes using the final model checkpoint, saved every 2,500 steps. The reward function in *Freeway* is sparse since the agent is only rewarded when it completely crosses the road. This poses an exploration problem for newly initialized agents because a random policy will almost surely never obtain a non-zero reward with a 100k frames budget. Inspired by the trick in IRIS [9], we opted for the simpler strategy of having a fixed epsilon-greedy parameter and using the policy. However, we reduced the sampling temperature from 1 to 0.0001 in *Freeway*, in order to avoid random walks that would not be conducive to learning in the early stages of training. The human-normalized score is calculated as  $\tau = \frac{A - R}{H - R}$ , where  $A$  is the agent's score,  $R$  is the score of a random policy, and  $H$  represents the average human score [5]. To determine  $H$ , the human players undergo familiarization with the game under identical constraints. We compare DyMoDreamer with state-of-the-art model-based RL methods, including OC-STORM [21], DreamerV3 [14], HarmonyDream [44], and DIAMOND [24]. The task scores are shown in Table 2 and the curves are shown in Figure 6.

Table 2: Game scores and overall human-normalized performance on the 26 games in the Atari 100k benchmark. Following the conventions of [14], scores within 5% of the best are highlighted in bold.

Game	Random	Human	STORM (2023)	OC-STORM (2025)	DIAMOND (2024)	DreamerV3 (2023)	Harmony DreamerV3	DyMoDreamer (ours)
Alien	228	7128	984	<b>1101</b>	744	<b>1118</b>	890	971
Amidar	6	1720	205	163	<b>226</b>	97	141	154.2
Assault	222	742	801	1270	<b>1526</b>	683	1003	902.1
Asterix	210	8503	1028	1754	<b>3698</b>	1062	1140	1195.5
Bank Heist	14	753	641	1075	20	398	1069	<b>1222.2</b>
Battle Zone	2360	37188	13540	4590	4702	<b>20300</b>	16456	16240
Boxing	0	12	80	<b>92</b>	87	82	80	<b>93.6</b>
Breakout	2	30	16	53	<b>132</b>	10	53	40.2
Chopper Command	811	7388	1888	<b>2090</b>	1370	2222	1510	740.4
Crazy Climber	10780	35829	66776	84111	<b>99168</b>	86225	82739	82569.4
Demon Attack	152	1971	165	411	288	<b>577</b>	203	248.3
Freeway	0	30	0	0	<b>33</b>	0	0	6.4
Frostbite	65	4335	1316	260	274	<b>3377</b>	679	722
Gopher	258	2413	8240	4457	5898	2160	<b>13043</b>	<b>13456.9</b>
Hero	1027	30826	11044	6441	5622	<b>13354</b>	<b>13378</b>	9874.1
James Bond	29	303	509	347	427	<b>540</b>	317	<b>541.8</b>
Kangaroo	52	3035	4208	4218	<b>5382</b>	2643	<b>5118</b>	4788.8
Krull	1598	2666	8413	<b>9715</b>	8610	8171	7754	<b>9624.8</b>
Kung Fu Master	256	22736	<b>26182</b>	<b>24988</b>	18714	<b>25900</b>	22274	<b>25641.4</b>
Ms Pacman	307	6952	<b>2673</b>	2401	1958	1521	1681	1838.6
Pong	-21	15	11	<b>20.6</b>	<b>20</b>	-4	19	<b>20.9</b>
Private Eye	25	69571	<b>7781</b>	85	114	3238	2932	3041.7
Qbert	164	13455	<b>4522</b>	<b>4546</b>	<b>4499</b>	2921	3933	1736.1
Road Runner	12	7845	17564	<b>20482</b>	<b>20673</b>	19230	14646	<b>20971.8</b>
Seaquest	68	42055	525	712	551	<b>962</b>	665	591.8
Up N Down	533	11693	7985	6623	3856	<b>46910</b>	10874	22321.5
Human Mean	0%	100%	126.7%	134.8%	146%	125%	136.5%	<b>156.6%</b>
Human Median	0%	100%	58.4%	43.8%	37%	49%	67.1%	71.3%

## E.2 DeepMind Visual Control Suite Experiments

The DeepMind Visual Control Suite is a widely used benchmark for visual locomotion. We train and evaluate our DyMoDreamer on all 20 continuous control tasks where the agent receives only high-dimensional images as observations and has a budget of 1M environment steps. We evaluate the agent performance by conducting 100 evaluation episodes for the final checkpoint and obtained the average score. DyMoDreamer is compared with DreamerV3, TD-MPC2 [3], and TWISTER [41], which are recent model-based approaches applied to continuous control. The task scores are shown in Table 3 and the curves are shown in Figure 7.

The results demonstrate the effectiveness of DyMoDreamer on DMC visual tasks. Our method greatly unleash the potential of RSSM. Similar to the results in Atari 100k, DyMoDreamer benefits from the dynamic modulation and shows superior performance compared to DreamerV3 in environments where key objects are sparse and independent of each other.

## E.3 Crafter Benchmark Experiments

In the Crafter [42] benchmark, the agent’s goal is to solve as many tasks as possible, e.g. slaying mobs, crafting items, and managing health indicators during each episode. Regarding baselines, we compare DyMoDreamer with IRIS,  $\Delta$ -IRIS and DreamerV3, and evaluate each run by computing the average return over 100 test episodes every 1M frames, the curve is shown in Figure 8.

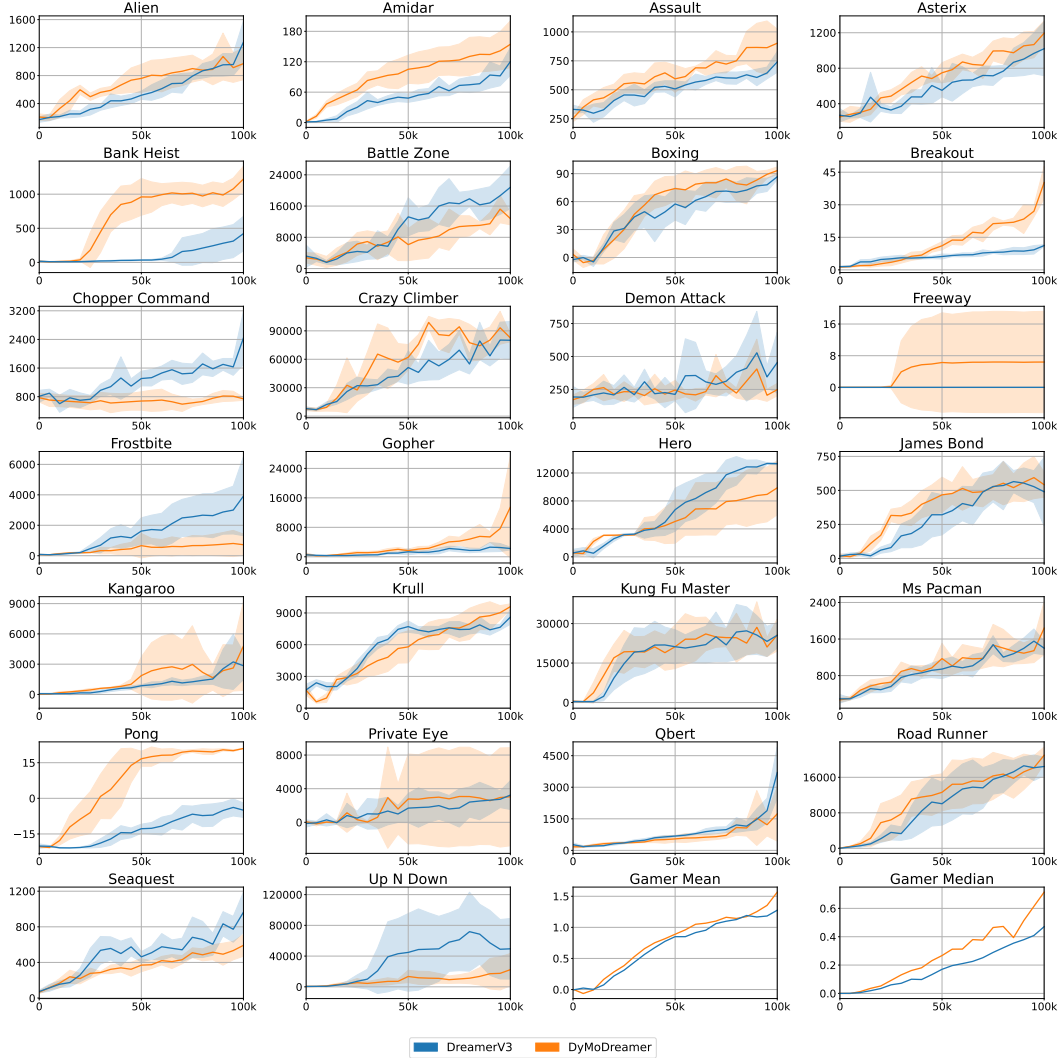


Figure 6: Evaluation curves of DyMoDreamer on the Atari 100k benchmark for individual games (400K environment steps). The solid lines represent the average scores over 5 seeds, and the filled areas indicate the standard deviation across these 5 seeds.

Table 3: Task scores and mean scores of baselines and our DyMoDreamer

Task	TD-MPC2 (2023)	TWISTER (2025)	DreamerV3 (2023)	DyMoDreamer (ours)
Environment steps	1M	1M	1M	1M
Acrobot Swingup	216	239	229	<b>447</b>
Ball In Cup Catch	717	967	<b>972</b>	967
Cartpole Balance	931	998	993	<b>999</b>
Cartpole Balance Sparse	<b>1000</b>	<b>1000</b>	964	999
Cartpole Swingup	808	819	861	<b>864</b>
Cartpole Swingup Sparse	739	735	759	<b>765</b>
Cheetah Run	550	694	836	<b>868.7</b>
Finger Spin	<b>986</b>	976	589	968
Finger Turn Easy	789	<b>924</b>	878	906
Finger Turn Hard	872	<b>910</b>	904	873
Hopper Hop	211	<b>314</b>	227	290
Hopper Stand	803	932	903	<b>943</b>
Pendulum Swingup	743	<b>832</b>	744	808.9
Quadruped Run	362	652	617	<b>770.4</b>
Quadruped Walk	253	<b>905</b>	811	792.0
Reacher Easy	<b>971</b>	933	951	896.8
Reacher Hard	<b>877</b>	566	<b>862</b>	821.9
Walker Run	728	711	684	<b>776.3</b>
Walker Stand	916	<b>977</b>	976	929.6
Walker Walk	945	951	961	<b>962.0</b>
Task mean	721	802	786	<b>832</b>
Task median	796	<b>908</b>	861	871

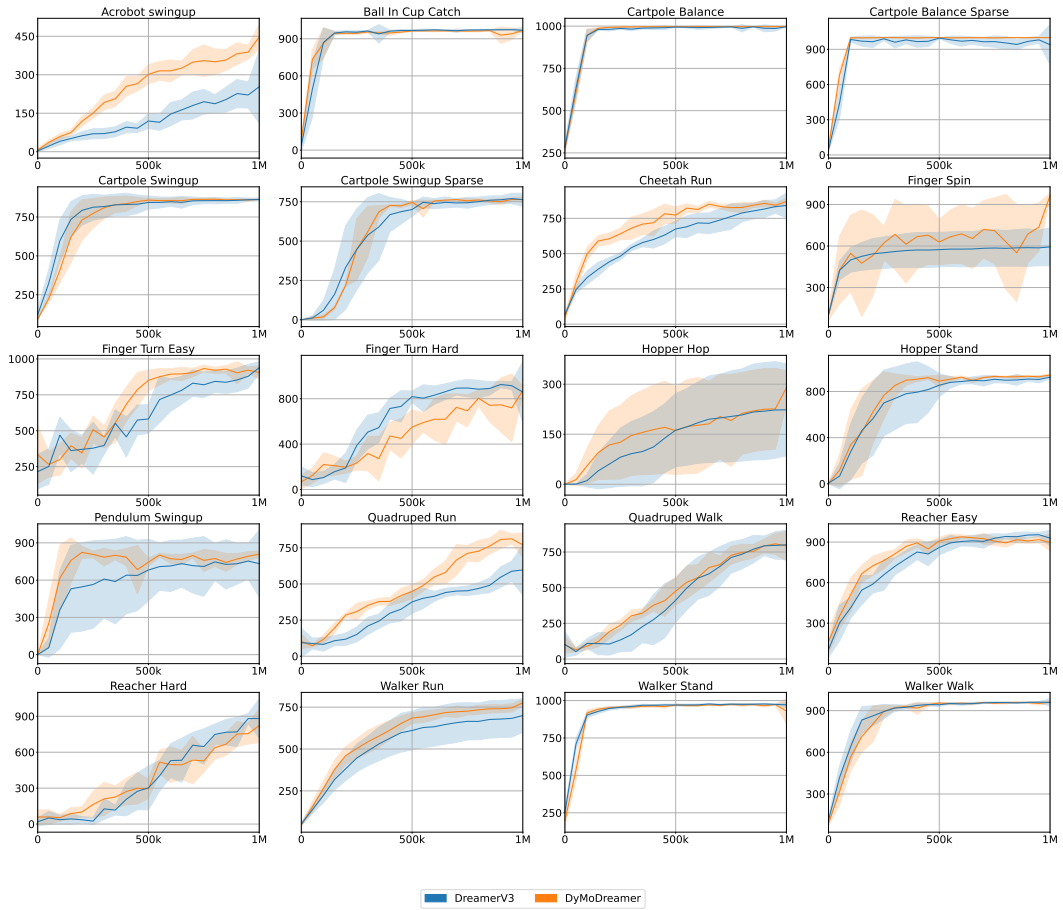


Figure 7: Evaluation curves of DyMoDreamer on the DMC suite. The solid lines represent the average scores over 5 seeds, and the filled areas indicate the standard deviation across these 5 seeds.

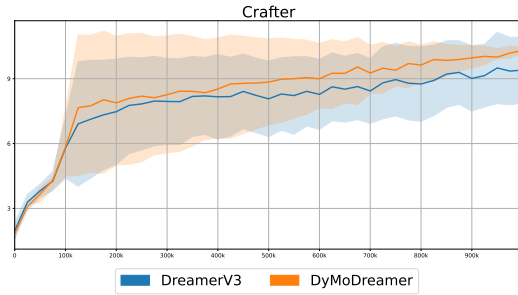


Figure 8: Evaluation curves of DyMoDreamer on the Crafter benchmark. The solid lines represent the average scores over 5 seeds, and the filled areas indicate the standard deviation across these 5 seeds.

## F Differential Observations

Figure 9, 10 and 11 illustrate the differential observations processed using differential mask constructed by Section 2.1. Compared to directly employing frame-wise differences, the masks generated through dilated convolutions capture dynamic objects more comprehensively, ensuring a more complete representation of motion-related features. Moreover, this demonstrates that the dynamic modulation is effectively encoded from the decision-related dynamic objects within the observations.

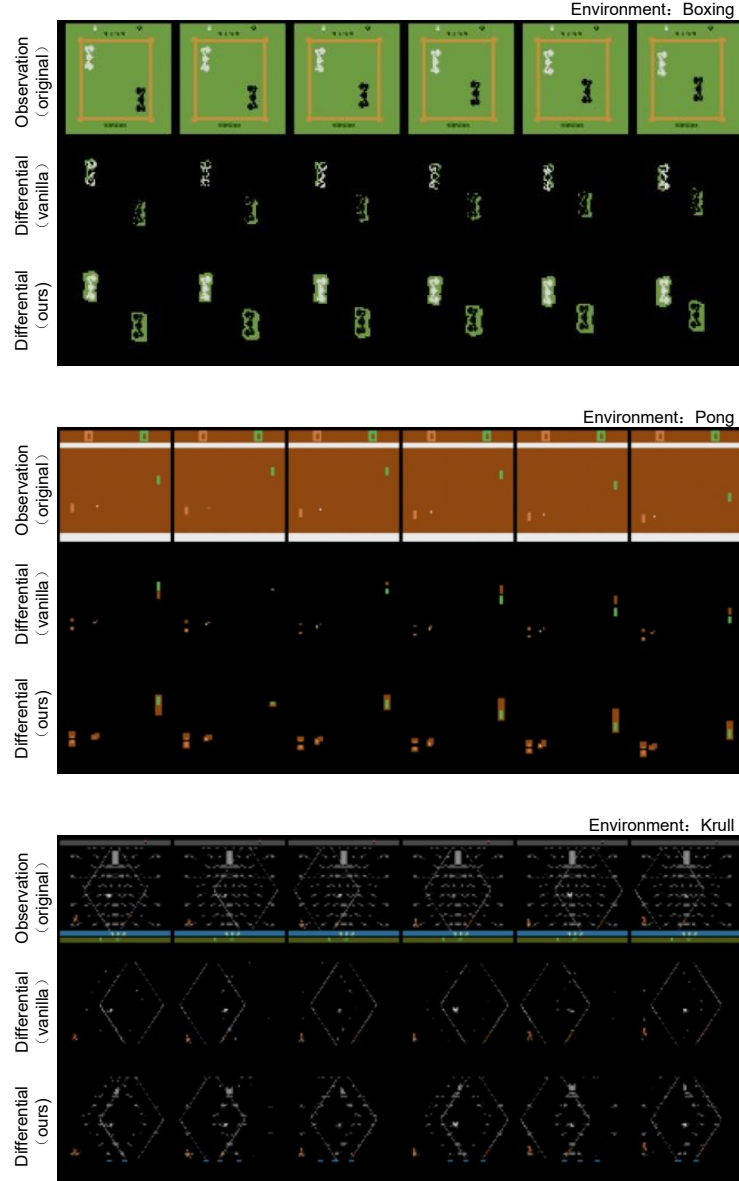


Figure 9: Differential observations for *Boxing* (the first subfigure), *Pong* (the second subfigure), and *Krull* tasks (the last subfigure). Each subfigure comprises three rows, and each illustrates a distinct form of observation. The first row displays the raw observations, the second row shows observations processed using vanilla frame differencing (2), and the third row presents the differential observations constructed using our proposed approach, which combines frame differencing with dilated convolutions.

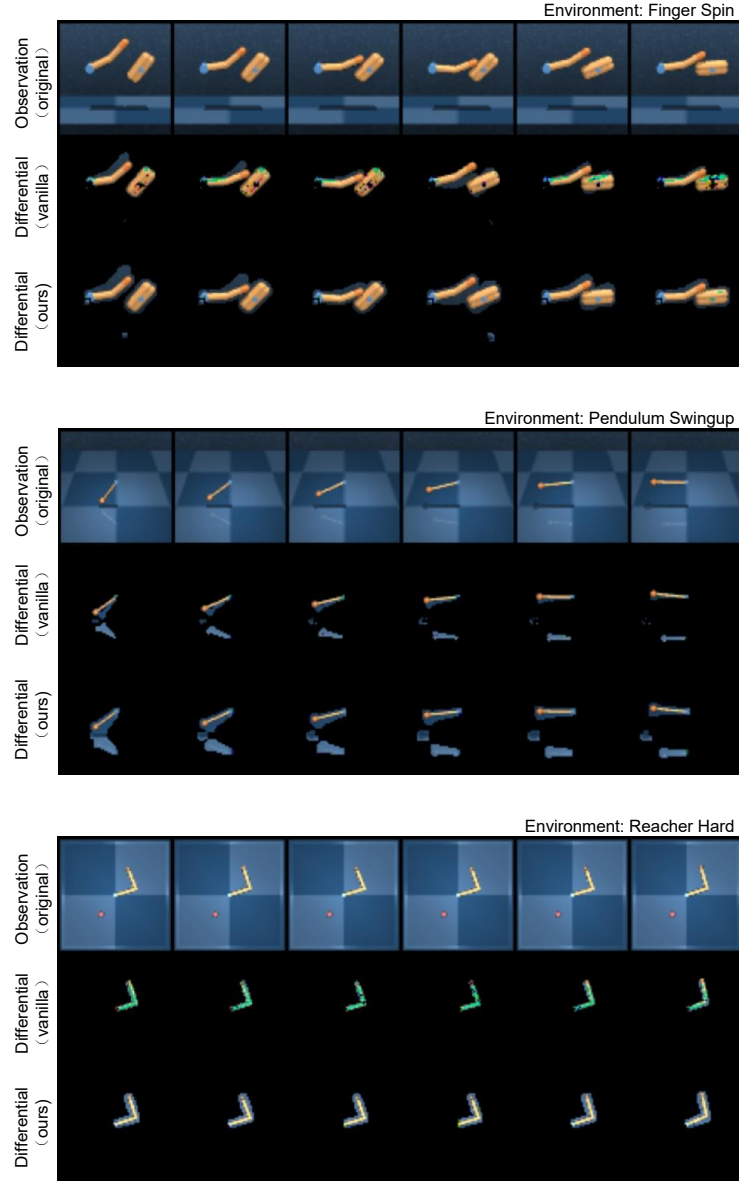


Figure 10: Differential observations for *Finger Spin* (the first subfigure), *Pendulum Swingup* (the second subfigure), and *Reacher Hard* (the last subfigure) tasks. Each subfigure comprises three rows, and each illustrates a distinct form of observation. The first row displays the raw observations, the second row shows observations processed using vanilla frame differencing (2), and the third row presents the differential observations constructed using our proposed approach, which combines frame differencing with dilated convolutions.

## G Alternative Differencing Strategies

A naive separation of dynamic and static components may introduce inductive biases in certain environments. To mitigate such issues (dynamic backgrounds or environmental noise), DyMoDreamer is designed to be highly flexible and accommodates a variety of differencing strategies, enabling seamless adaptation to diverse visual environments. While our default implementation adopts frame-wise pixel differencing to highlight dynamic cues, the architecture readily supports alternative formulations such as moving average difference, temporal skip differencing (Appendix K.6), or

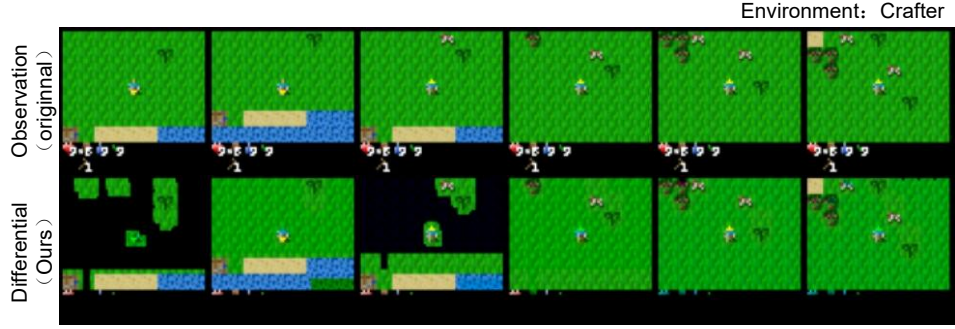


Figure 11: Differential observations for Crafter. The first row displays the raw observations, the second row presents the differential observations constructed using our proposed approach, which combines frame differencing with dilated convolutions.

multi-frames differencing. Importantly, frame differencing has long been recognized in computer vision as a lightweight yet effective method for motion detection, foreground segmentation, and event-based visual processing, due to its ability to isolate dynamic elements from static backgrounds [59]. By leveraging this principle within the context of world model, DyMoDreamer inherits its computational efficiency and interpretability, while maintaining the temporal information with the dynamic modulation mechanism. DyMoDreamer demonstrates that the differencing-based dynamic modulation not only enriches temporal representation but also offers a flexible interface to incorporate various differencing strategies, making it adaptable to a broad range of task scenarios.

**Moving Average Difference** We formally express the replacement of frame differencing (Equation 2) with moving average differencing as follows:

$$D(o_{i,h,w,c}) = \begin{cases} 1, & \text{if } \|o_{i,h,w,c} - \text{avg}_i\|_2 > \epsilon \\ 0, & \text{others} \end{cases} \quad (16)$$

where  $\text{avg}_i$  is defined as:

$$\text{avg}_i = \begin{cases} \frac{1}{l} \sum_{k=i-l}^{i-1} o_{k,h,w,c} & \text{if } i \geq l \\ \frac{1}{i} \sum_{k=0}^{i-1} o_{k,h,w,c} & \text{if } i \leq l \end{cases} \quad (17)$$

where  $l$  is the temporal averaging window size. This approach demonstrates superior performance over naive frame differencing in egocentric vision tasks, as evidenced in domains like *Battlezone* (Table 6).

**Multi-frame Logical Differencing** We further propose a novel multi-frame logical-relational differencing that stabilizes the differencing output  $D(o_{i,h,w,c})$  in Equation 2 by applying logical AND operations (that is, only pixels whose masks were 1 in the past few times will be displayed as 1 in the final matrix.) across temporally displaced frames:

$$D_{\log}(o_{i,h,w,c}) = \bigwedge_{k \in \Omega(t)} D_k, \quad (18)$$

where  $\Omega(t) = \{i - \Delta, i\}$  and  $\Delta$  is the symmetric temporal window size. This method demonstrates superior performance in environments with higher temporal continuity, as evidenced in domains like (Table 6).

Table 4: DyMoDreamer with different differencing strategies.

DyMoDreamer			
	Moving Average Differencing	Multi-frame Logical Differencing	Vanilla
Battle Zone	<b>20351</b>	-	16240
Road Runner	-	<b>21378</b>	20972

## H Static Factors

We extend DyMoDreamer by introducing a dedicated decoder for its stochastic representations  $z_t$ , revealing an emergent specialization in the learned latent space:

$$\begin{aligned}
 \text{Stochastic encoder:} \quad & z_t \sim q_\phi(z_t | h_t, o_t) \\
 \text{Dynamic encoder:} \quad & d_t \sim q_\phi(d_t | h_t, o'_t) \\
 \text{Decoder:} \quad & \hat{dyn}_t = p_\phi(\hat{dyn}_t | h_t, z_t, d_t) \\
 \text{Static decoder:} \quad & \hat{sta}_t = p_\phi(\hat{sta}_t | h_t, z_t).
 \end{aligned} \tag{19}$$

The reconstructed observations  $\hat{o}_t$  is calculated by:

$$\hat{o}_t = \hat{dyn}_t + \hat{sta}_t. \tag{20}$$

Critically, we maintain the original end-to-end loss 5 without modification, and validate the representational specialization through natural reconstructions, which is shown in Figure 12. The results demonstrate a clear representational dissociation: stochastic representations encoding predominantly capture static environmental factors and passive dynamics (e.g., static backgrounds and the black NPC in *Boxing*), while the dynamic modulation features specialize in agent-controllable elements (e.g., the controlled white player in *Boxing*). This emergent specialization suggests an natural segregation within the model’s representational architecture like the denoised Markov decision process [60], since we do not explicitly assign reconstruction targets to different decoders.

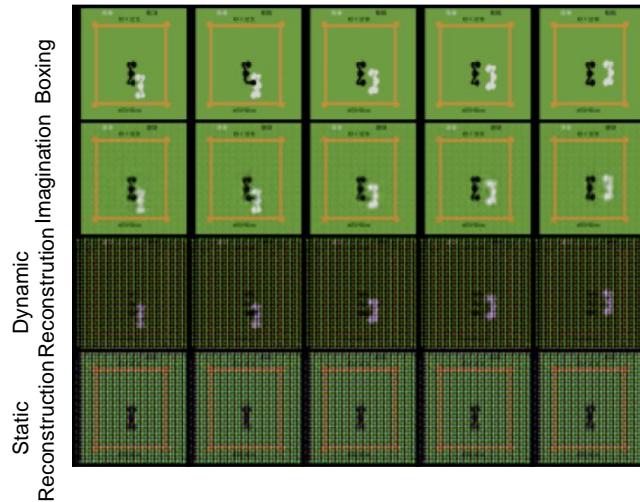


Figure 12: The first row shows ground-truth trajectories under the same action sequence. The second row presents imagined trajectories reconstructed from the predicted priors. The third row shows dynamic decoding results based on dynamically modulated features  $d_t$ . The fourth row shows static decoding results based on stochastic representations  $z_t$ .

## I Applicability beyond Images

To evaluate the applicability of DyMoDreamer in state-based environments, we conducted experiments on DeepMind Proprio—a proprioceptive control benchmark where observations consist of structured state vectors such as velocity and position. In this setting, observation differencing naturally reduces to state differencing, with temporal dynamics being more explicitly encoded. Consequently, differential modulation provides similar benefits in non-visual settings, since such differences also carry meaningful physical semantics similar to the differential observations—for instance, differential positions implicitly encode velocity, while the differential velocities reflect acceleration.

Table 5: Game scores in the DeepMind Proprio benchmark.

	DreamerV3	DyMoDreamer
Acrobot Swingup	134	<b>225</b>
Cheetah Run	614	<b>625</b>
Swingup	<b>931</b>	<b>932</b>

## J Generality

To further validate the effectiveness of our dynamic modulation mechanism, we integrated it into STORM [25], a recent efficient transformer-based world model. As shown in the results below, this integration also leads to clear performance gain.

Table 6: Game scores in the DeepMind Proprio benchmark.

	STORM (Reproduced)	DyMoDreamer
Boxing	81	<b>85</b>
Krull	6824	<b>8563</b>
Pong	18	<b>19.1</b>
RoadRunner	13866	<b>19337</b>

## K Ablations

In the following, we provide additional ablation studies to explore the effect of different components of DyMoDreamer. We conduct all ablations on four games: (i) *Krull*, a game that features multiple levels, with small and numerous dynamic objects, (ii) *Boxing*, a game with a single level and characterized by large and sparse dynamic objects, (iii) *Pong*, a game with a single level and characterized by small and sparse dynamic objects. (iv) *Road Runner*, a game with both small and large dynamic objects. We use the same hyperparameters as described in Appendix L for all ablations. The aggregated ablation table 7 summarizing the performance of different ablation studies.

Table 7: Game scores in the DeepMind Proprio benchmark.

Ablation Variant	Boxing	Krull	Pong	Road Runner
DyMoDreamer	93.6	9624.8	20.9	20971.8
Removing dynamic modulation	80	7969	18.5	12536
Removing $\mathcal{L}_{\text{reg}}$	90	8961	20	20918
High-dimensional (48x48)	76	7325	18.2	16320
With differential reconstruction	71	7895	19.9	17323
Latent difference	81	7855	20	12266
Low-dimensional $z_t$ (16x16)	73	7423	19	17465

### K.1 High-dimensional Stochastic Representations

Scaling to larger models leads to higher data efficiency and episode rewards [61]. For example, in TDMPC2 [3], a larger parameter count leads to improved results in the Meta-World [62] and DeepMind Control (DMC) [63] environments. Therefore, we compare the vanilla DreamerV3 that extends  $z_t$  to 48 categories with 48 classes for the sake of fairness.

The result is shown in Figure 13, which reveals that only the dimension added in vanilla DreamerV3  $z_t$  do not achieve the same performance as DyMoDreamer. This once again indicates that dynamic modulation is not equivalent to simply increasing dimensions but rather enriching the information used by agents for decision making.

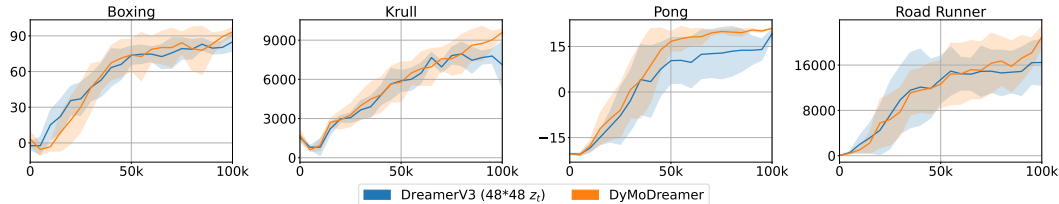


Figure 13: Ablation studies on the high-dimensional DreamerV3.

### K.2 Reconstruction of Differential Observations

To improve the world model’s focus on reward-relevant objects, OC-STORM introduces an additional object-centric model, Cutie [54], based on target segmentation. This enhancement significantly improves the baseline STORM’s performance. OC-STORM encodes both raw and object-centric observations to obtain stochastic representations and reconstructs these separately during the autoregressive prediction process to train the VAEs. Following a similar approach, we conduct an ablation study on reconstructing differential observations in DyMoDreamer, with results shown in Figure 14. Specifically, we introduce an additional term  $\mathcal{L}_{\text{dif}}(\phi) = -\ln p_\phi(o'_t | h_t, d_t)$  into the prediction loss function (6). Furthermore, we incorporate a dynamic decoder into (3):

$$\text{Dynamic decoder: } \hat{o}'_t = p_\phi(\hat{o}'_t | h_t, d_t). \quad (21)$$

Figure 14 shows that adding a dynamic decoder does not improve DyMoDreamer’s performance. Instead, it weakens dynamic modulation’s effectiveness and significantly increases computational

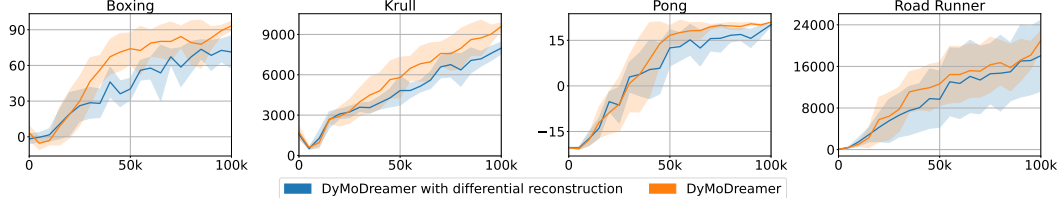


Figure 14: Ablation study on differential observation reconstruction. Adding a dynamic decoder does not improve performance and increases computational cost.

cost. This is because differential observations are not strictly edge segmentations. Their primary function is to isolate and encode dynamic features of the environment rather than improving its reconstruction.

The substantial improvement observed in the *Pong* environment suggests that when dynamic objects are both small and sparse, differential observations serve as a relatively accurate reconstruction target, allowing the agent to match the performance of pre-trained visual models with a faster speed. Explicitly constraining the dynamic modulators with a decoder may actually degrade performance due to coarse reconstruction targets. In contrast, implicitly training stochastic representations and dynamic modulators together within a single decoder is more efficient and yields better performance. We claim once again that the goal of dynamic modulation is not to improve the reconstruction accuracy, but to enable the agent to leverage richer dynamic information for decision making.

### K.3 Modulation with Latent Difference

We conducted additional experiments using latent-space differencing in place of our dynamic modulation mechanism. The latent difference [30] in MFRL is defined as  $\delta_t = z_t - z_{t-1}$ , where  $z_t$  and  $z_{t-1}$  are latent features extracted at consecutive time steps by the same encoder. Similarly, we also experimented with using  $\delta_t$  in place of  $d_t$  as input to the sequencemodel  $f_\phi$ . In this setting, the sequence model is changed into:

$$\text{Sequence model: } h_t = f_\phi(h_{t-1}, z_{t-1}, \delta_{t-1}, a_{t-1}), \quad (22)$$

where the dynamic modulation is retained, coming from  $\delta_t$  but not the dynamic modulators  $d_t$ . Both the computation and encoding of differential observations are removed. The results show that this approach fails to match DyMoDreamer’s performance, particularly in environments like *Road Runner*, where the critical objects occupy minimal pixels (e.g., the seed and steel occupying just 1 pixel). This occurs because: (1) The original encoding’s precision limits small dynamic feature capture. (2) The categorical distributions in latent space lose fine-grained positional information. (3) Without the explicit dynamic modulation based on differential observations, frame-to-frame differences of small objects become unreliable. DyMoDreamer’s strength lies in its hybrid approach combining pixel-level dynamic detection with latent categorical encoding, which preserves critical small-scale dynamics while filtering noise.

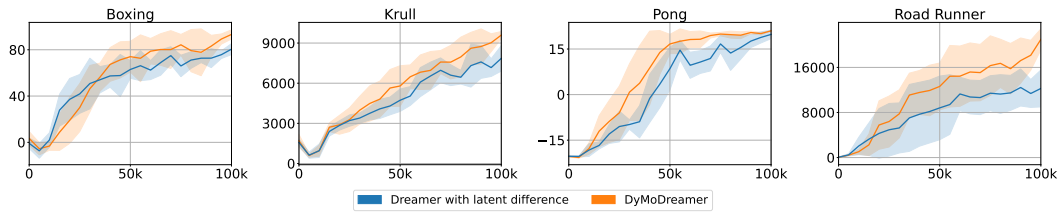


Figure 15: Ablation study on latent difference RSSM.

We emphasize again that DyMoDreamer is fundamentally different from the latent flow, despite both being inspired by the general idea of differencing. DyMoDreamer separates the representation pathways: the dynamic modulator  $d_t$  and the stochastic representation  $z_t$  are derived from two different encoders (Equation 1). Specifically,  $z_t$  is encoded from the full observations  $o_t$ , while  $d_t$  is encoded from the differential observations  $o'_t$  derived from the frame-differencing and processed

by a distinct dynamic encoder. Due to the characteristics of CNNs, the encoding of differential observations is not equal to the difference between stochastic representations:

$$z_t - z_{t-1} \neq d_t \sim q_\phi(d_t | h_t, o'_t), \quad (23)$$

where the dynamic modulation mechanism allows DyMoDreamer to retain subtle yet decision-critical dynamic cues that might be overlooked by  $z_t$  and  $z_{t-1}$  alone.

#### K.4 DyMoDreamer with Harmonious Loss

An intriguing question is whether the inclusion of additional loss terms or adjustments to existing ones during the training of the world model impacts its effectiveness. The answer is unequivocally yes: even without introducing new loss terms, modifying the weights of existing ones can significantly influence the model's performance [44]. Recent advances, such as HarmonyDream [44], highlight the benefits of adaptively adjusting the weights of different loss terms during training. By employing a harmonious loss framework [64], this approach achieves performance superior to that of the vanilla DreamerV3. In this section we provide a detailed discussion on the impact of incorporating harmonious loss within DyMoDreamer, demonstrating its potential for improved training efficiency and effectiveness. Adjusting the coefficients of different loss terms has the potential to significantly enhance the performance of world-model-based reinforcement learning algorithms [44]. For DyMoDreamer, compared to DreamerV3, we add three additional loss terms during the training of the world model, further complicating the challenge of tuning the initial loss coefficients. To address this, we adopt a harmonious loss strategy inspired by HarmonyDream [44], dynamically adjusting the dominance between the observation and the reward modeling during world model training process. In this section, we explore the impact of this approach on the performance of DyMoDreamer.

To simplify the presentation and avoid excessive complexity, we consider the vanilla end-to-end loss as below:

$$\begin{aligned} \mathcal{L}(\phi) = & \omega_{\text{img}} \mathcal{L}_{\text{rec}}(\phi) + \omega_{\text{rew}} \mathcal{L}_{\text{rew}}(\phi) + \omega_{\text{con}} \mathcal{L}_{\text{con}}(\phi) + \omega_{\text{dyn}} \mathcal{L}_{\text{dyn}}(\phi) \\ & + \omega_{\text{rep}} \mathcal{L}_{\text{rep}}(\phi) + \omega_{\text{reg}} \mathcal{L}_{\text{reg}}(\phi). \end{aligned} \quad (24)$$

Then the harmonious loss is constructed as:

$$\mathcal{L}_h(\phi, \omega_i) = \sum \frac{1}{\omega_i} \mathcal{L}_i + \ln(1 + \omega_i) \quad (25)$$

where  $i \in \{\text{img, rew, con, dyn, rep, reg}\}$ , and specifically, inspired by HarmonyDreamer, we recombine the dynamics and representation losses into  $\mathcal{L}_d(\phi)$  as follows:

$$\mathcal{L}_d(\phi) = \alpha \mathcal{L}_{\text{dyn}}(\phi) + (1 - \alpha) \mathcal{L}_{\text{rep}}(\phi). \quad (26)$$

And  $\alpha$  is the KL balancing coefficient predefined the same as (5). The reason why we use  $\ln(1 + \omega_i)$  as regularization terms is that  $\omega_i$  is parameterized as  $\omega_i = \exp(\omega_i) > 0$  to optimize parameters  $\omega_i$  free of sign constraint. Since a loss item with small values, such as the reward loss, can lead to extremely large coefficient  $1/\omega_i \approx L - 1 \gg 1$ , which potentially hurt training stability. The derivation of the harmonious loss scale is as follows.

To minimize  $\mathbb{E}[\mathcal{L}_h(\phi, \omega_i)]$ , we force the the partial derivative w.r.t.  $\omega_i$  to 0:

$$\begin{aligned} \nabla_\omega \mathbb{E}[\mathcal{L}_h(\phi, \omega)] &= \nabla_\omega \left( \frac{1}{\omega} \mathbb{E}[\mathcal{L}] + \ln(1 + \omega) \right) = -\frac{1}{\omega^2} \mathbb{E}[\mathcal{L}] + \frac{1}{1 + \omega} \\ \omega^* &= \frac{\mathbb{E}[\mathcal{L}] + \sqrt{\mathbb{E}[\mathcal{L}]^2 + 4\mathbb{E}[\mathcal{L}]}}{2}. \end{aligned} \quad (27)$$

Therefore the learnable loss weight, in the rectified harmonious loss, approximates the analytic loss weight:

$$\frac{1}{\omega^*} = \frac{2}{\mathbb{E}[\mathcal{L}] + \sqrt{\mathbb{E}[\mathcal{L}]^2 + 4\mathbb{E}[\mathcal{L}]}} \quad (28)$$

and equivalently, the harmonized loss scale is:

$$\mathbb{E}\left[\frac{\mathcal{L}}{\omega^*}\right] = \frac{2}{1 + \sqrt{1 + \frac{4}{\mathbb{E}[\mathcal{L}]}}} < 1, \quad (29)$$

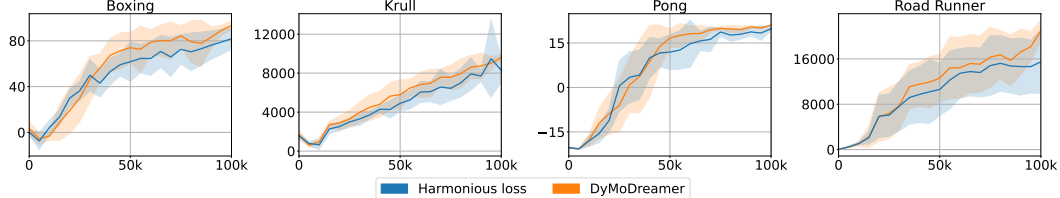


Figure 16: Ablation studies on DyMoDreamer with harmonious loss.

and add the regularization term  $\ln(1 + \omega_i)$  results in the  $4/\mathbb{E}[\mathcal{L}]$  in the  $\sqrt{1 + 4/\mathbb{E}[\mathcal{L}]}$  term, which prevents the loss weight from getting extremely large when faced with a small  $\mathbb{E}[\mathcal{L}]$ . Regrettably, Figure 16 indicates that while the harmonious loss achieves performance comparable to fixed parameters only in the *Pong* task, but falls short in *Krull*, *Boxing* and *Road Runner* tasks. A potential explanation for this discrepancy is the increased complexity introduced by additional loss terms. The learning rate inherited from the original settings may no longer be optimal, as it appears overly aggressive for adapting the harmonious coefficients.

### K.5 Dimensions of the Dynamic Modulation

The proportion of dynamic objects varies significantly across tasks, as evidenced by the differential mask rate. For instance, in the *Pong* task, the average mask rate (AMR) for a single episode reaches as high as 98.5%, reflecting the minimal volume of dynamic components. In contrast, the AMRs for single episodes in *Boxing* and *Krull* tasks are 94.3% and 83.1%, respectively, due to the larger proportion of dynamic elements in these environments. Consequently, the different dimensionality of  $d_t$  can significantly impact the performance of world models. For instance, OC-STORM treats the number of objects as a hyperparameter, and manually adjustis it for different tasks. This task-specific modification results in varying dimensions of the stochastic encoding output by the visual model, which partially enhances OC-STORM’s performance [21]. Furthermore, the relative size between  $z_t$  and  $d_t$  could also influences performance. Increasing the dimension of  $d_t$  effectively enlarges the latent variable space, potentially introducing redundant information that could hinder the agent’s decision-making process.

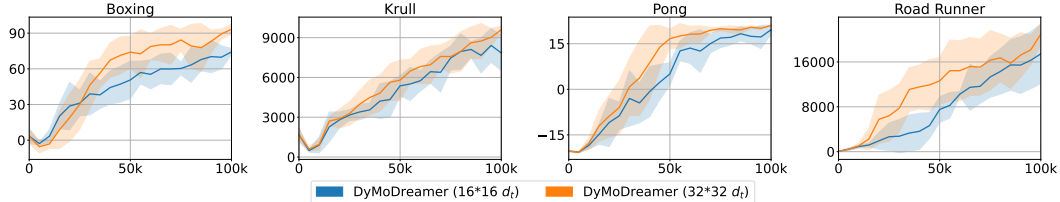


Figure 17: Ablation studies on the dimension of dynamic modulation.

The results in Figure 17 indicate that using  $16 \times 16$  classified dynamic modulators does not fully encode the dynamic information from the differential observations. In other words, low-dimensional dynamic modulation fails to accurately integrate dynamic information into the RSSM, thereby not enriching the decision-making process.

### K.6 Longer Difference Interval

Although using single-frame differences already yields substantial performance improvements, we include an ablation study on the difference interval  $k$  in this section. Specifically, we set  $k = 3$  to evaluate DyMoDreamer, and present the results in Figure 18.

The results show that using a longer differencing interval encourages the world model to focus on longer-term changes rather than transient noise or local perturbations. This often leads to better performance in smoother environments, but may fail to capture critical dynamics occurring in intermediate frames, such as the rapid punching in *Boxing*.

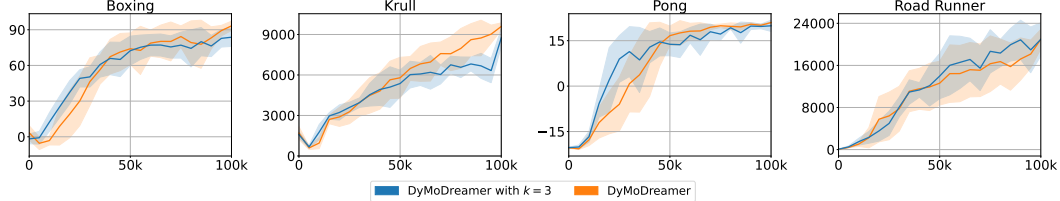


Figure 18: Ablation studies on  $k = 3$ .

## L Hyperparameters

Table 8 details the hyperparameters of the optimization and environment, as well as hyperparameters shared by multiple components. The environment will provide a “done” signal when losing a life, but will continue running until the actual reset occurs.

Table 8: Hyperparameters

Name	Value
<b>General</b>	
Batch size	16
Batch length	64
Activation	LayerNorm + SiLU
Optimizer	Adam
<b>World Model</b>	
Learning rate	$10^{-4}$
Adam epsilon	$10^{-8}$
Gradient clipping	1000
<b>Actor Critic</b>	
Imagination horizon	15
Discount horizon	333
Return lambda	0.95
Critic EMA decay	0.98
Critic EMA regularizer	1
Actor entropy scale	$3 \times 10^{-4}$
Learning rate	$3 \times 10^{-5}$
Adam epsilon	$10^{-5}$
Gradient clipping	100

## NeurIPS Paper Checklist

### 1. Claims

Question: Do the main claims made in the abstract and introduction accurately reflect the paper's contributions and scope?

Answer: **[Yes]**

Justification: All claims made in the title, abstract and introduction are limited to the paper's scope, and match our results in Section 3. We include a motivational example from the infant cognition in the introduction but it is clear that this scenario is motivational and not addressed by the paper.

Guidelines:

- The answer NA means that the abstract and introduction do not include the claims made in the paper.
- The abstract and/or introduction should clearly state the claims made, including the contributions made in the paper and important assumptions and limitations. A No or NA answer to this question will not be perceived well by the reviewers.
- The claims made should match theoretical and experimental results, and reflect how much the results can be expected to generalize to other settings.
- It is fine to include aspirational goals as motivation as long as it is clear that these goals are not attained by the paper.

### 2. Limitations

Question: Does the paper discuss the limitations of the work performed by the authors?

Answer: **[Yes]**

Justification: We discuss the limitations of our work in a separate "Limitations" section (see Section B), and analyze the trade-offs in computational efficiency in Section 3.2.

Guidelines:

- The answer NA means that the paper has no limitation while the answer No means that the paper has limitations, but those are not discussed in the paper.
- The authors are encouraged to create a separate "Limitations" section in their paper.
- The paper should point out any strong assumptions and how robust the results are to violations of these assumptions (e.g., independence assumptions, noiseless settings, model well-specification, asymptotic approximations only holding locally). The authors should reflect on how these assumptions might be violated in practice and what the implications would be.
- The authors should reflect on the scope of the claims made, e.g., if the approach was only tested on a few datasets or with a few runs. In general, empirical results often depend on implicit assumptions, which should be articulated.
- The authors should reflect on the factors that influence the performance of the approach. For example, a facial recognition algorithm may perform poorly when image resolution is low or images are taken in low lighting. Or a speech-to-text system might not be used reliably to provide closed captions for online lectures because it fails to handle technical jargon.
- The authors should discuss the computational efficiency of the proposed algorithms and how they scale with dataset size.
- If applicable, the authors should discuss possible limitations of their approach to address problems of privacy and fairness.
- While the authors might fear that complete honesty about limitations might be used by reviewers as grounds for rejection, a worse outcome might be that reviewers discover limitations that aren't acknowledged in the paper. The authors should use their best judgment and recognize that individual actions in favor of transparency play an important role in developing norms that preserve the integrity of the community. Reviewers will be specifically instructed to not penalize honesty concerning limitations.

### 3. Theory assumptions and proofs

Question: For each theoretical result, does the paper provide the full set of assumptions and a complete (and correct) proof?

Answer: [NA]

Justification: We do not have novel theoretical results, but instead apply the existing theoretical framework of dynamic modulation to world modeling. Section 2 provides the necessary theoretical background to dynamic modulation for world modeling in a clearly stated and referenced way.

Guidelines:

- The answer NA means that the paper does not include theoretical results.
- All the theorems, formulas, and proofs in the paper should be numbered and cross-referenced.
- All assumptions should be clearly stated or referenced in the statement of any theorems.
- The proofs can either appear in the main paper or the supplemental material, but if they appear in the supplemental material, the authors are encouraged to provide a short proof sketch to provide intuition.
- Inversely, any informal proof provided in the core of the paper should be complemented by formal proofs provided in appendix or supplemental material.
- Theorems and Lemmas that the proof relies upon should be properly referenced.

#### 4. Experimental result reproducibility

Question: Does the paper fully disclose all the information needed to reproduce the main experimental results of the paper to the extent that it affects the main claims and/or conclusions of the paper (regardless of whether the code and data are provided or not)?

Answer: [Yes]

Justification: We provide all the necessary details to reproduce our results. Our method is explained in Section 3, with the full training procedure detailed in Appendix E. We provide full details of hyperparameters in Appendix L, and reinforcement learning objectives in Appendix D. Additionally our entire codebase will be open-source, and is shown in the supplementary material.

Guidelines:

- The answer NA means that the paper does not include experiments.
- If the paper includes experiments, a No answer to this question will not be perceived well by the reviewers: Making the paper reproducible is important, regardless of whether the code and data are provided or not.
- If the contribution is a dataset and/or model, the authors should describe the steps taken to make their results reproducible or verifiable.
- Depending on the contribution, reproducibility can be accomplished in various ways. For example, if the contribution is a novel architecture, describing the architecture fully might suffice, or if the contribution is a specific model and empirical evaluation, it may be necessary to either make it possible for others to replicate the model with the same dataset, or provide access to the model. In general, releasing code and data is often one good way to accomplish this, but reproducibility can also be provided via detailed instructions for how to replicate the results, access to a hosted model (e.g., in the case of a large language model), releasing of a model checkpoint, or other means that are appropriate to the research performed.
- While NeurIPS does not require releasing code, the conference does require all submissions to provide some reasonable avenue for reproducibility, which may depend on the nature of the contribution. For example
  - (a) If the contribution is primarily a new algorithm, the paper should make it clear how to reproduce that algorithm.
  - (b) If the contribution is primarily a new model architecture, the paper should describe the architecture clearly and fully.
  - (c) If the contribution is a new model (e.g., a large language model), then there should either be a way to access this model for reproducing the results or a way to reproduce the model (e.g., with an open-source dataset or instructions for how to construct the dataset).

(d) We recognize that reproducibility may be tricky in some cases, in which case authors are welcome to describe the particular way they provide for reproducibility. In the case of closed-source models, it may be that access to the model is limited in some way (e.g., to registered users), but it should be possible for other researchers to have some path to reproducing or verifying the results.

## 5. Open access to data and code

Question: Does the paper provide open access to the data and code, with sufficient instructions to faithfully reproduce the main experimental results, as described in supplemental material?

Answer: [Yes]

Justification: The environments we consider are open-source, and we provide our codes and results in the the supplementary material.

Guidelines:

- The answer NA means that paper does not include experiments requiring code.
- Please see the NeurIPS code and data submission guidelines (<https://nips.cc/public/guides/CodeSubmissionPolicy>) for more details.
- While we encourage the release of code and data, we understand that this might not be possible, so “No” is an acceptable answer. Papers cannot be rejected simply for not including code, unless this is central to the contribution (e.g., for a new open-source benchmark).
- The instructions should contain the exact command and environment needed to run to reproduce the results. See the NeurIPS code and data submission guidelines (<https://nips.cc/public/guides/CodeSubmissionPolicy>) for more details.
- The authors should provide instructions on data access and preparation, including how to access the raw data, preprocessed data, intermediate data, and generated data, etc.
- The authors should provide scripts to reproduce all experimental results for the new proposed method and baselines. If only a subset of experiments are reproducible, they should state which ones are omitted from the script and why.
- At submission time, to preserve anonymity, the authors should release anonymized versions (if applicable).
- Providing as much information as possible in supplemental material (appended to the paper) is recommended, but including URLs to data and code is permitted.

## 6. Experimental setting/details

Question: Does the paper specify all the training and test details (e.g., data splits, hyperparameters, how they were chosen, type of optimizer, etc.) necessary to understand the results?

Answer: [Yes]

Justification: We provide all hyperparameters, including environment configurations, number of epochs, batch sizes, data collection schedules, optimizer settings, architectures and reinforcement learning details in Appendices.

Guidelines:

- The answer NA means that the paper does not include experiments.
- The experimental setting should be presented in the core of the paper to a level of detail that is necessary to appreciate the results and make sense of them.
- The full details can be provided either with the code, in appendix, or as supplemental material.

## 7. Experiment statistical significance

Question: Does the paper report error bars suitably and correctly defined or other appropriate information about the statistical significance of the experiments?

Answer: [Yes]

Justification: We follow the official evaluation protocol provide confidence intervals for our experimental result.

Guidelines:

- The answer NA means that the paper does not include experiments.
- The authors should answer "Yes" if the results are accompanied by error bars, confidence intervals, or statistical significance tests, at least for the experiments that support the main claims of the paper.
- The factors of variability that the error bars are capturing should be clearly stated (for example, train/test split, initialization, random drawing of some parameter, or overall run with given experimental conditions).
- The method for calculating the error bars should be explained (closed form formula, call to a library function, bootstrap, etc.)
- The assumptions made should be given (e.g., Normally distributed errors).
- It should be clear whether the error bar is the standard deviation or the standard error of the mean.
- It is OK to report 1-sigma error bars, but one should state it. The authors should preferably report a 2-sigma error bar than state that they have a 96% CI, if the hypothesis of Normality of errors is not verified.
- For asymmetric distributions, the authors should be careful not to show in tables or figures symmetric error bars that would yield results that are out of range (e.g. negative error rates).
- If error bars are reported in tables or plots, The authors should explain in the text how they were calculated and reference the corresponding figures or tables in the text.

## 8. Experiments compute resources

Question: For each experiment, does the paper provide sufficient information on the computer resources (type of compute workers, memory, time of execution) needed to reproduce the experiments?

Answer: [\[Yes\]](#)

Justification: We detail the type of GPU, memory and time of execution in Section 3.2.

Guidelines:

- The answer NA means that the paper does not include experiments.
- The paper should indicate the type of compute workers CPU or GPU, internal cluster, or cloud provider, including relevant memory and storage.
- The paper should provide the amount of compute required for each of the individual experimental runs as well as estimate the total compute.
- The paper should disclose whether the full research project required more compute than the experiments reported in the paper (e.g., preliminary or failed experiments that didn't make it into the paper).

## 9. Code of ethics

Question: Does the research conducted in the paper conform, in every respect, with the NeurIPS Code of Ethics <https://neurips.cc/public/EthicsGuidelines>?

Answer: [\[Yes\]](#)

Justification: We do not foresee any harms caused by the research process (there are no human subjects involved in our work, and the environments we use are open-source), and we also do not foresee any direct harmful societal impact of our work.

Guidelines:

- The answer NA means that the authors have not reviewed the NeurIPS Code of Ethics.
- If the authors answer No, they should explain the special circumstances that require a deviation from the Code of Ethics.
- The authors should make sure to preserve anonymity (e.g., if there is a special consideration due to laws or regulations in their jurisdiction).

## 10. Broader impacts

Question: Does the paper discuss both potential positive societal impacts and negative societal impacts of the work performed?

Answer: [\[Yes\]](#)

Justification: : Our introduction discuss the general motivation for our research, and position it into a broader picture. We consider both positive and negative societal impacts in Section C.

Guidelines:

- The answer NA means that there is no societal impact of the work performed.
- If the authors answer NA or No, they should explain why their work has no societal impact or why the paper does not address societal impact.
- Examples of negative societal impacts include potential malicious or unintended uses (e.g., disinformation, generating fake profiles, surveillance), fairness considerations (e.g., deployment of technologies that could make decisions that unfairly impact specific groups), privacy considerations, and security considerations.
- The conference expects that many papers will be foundational research and not tied to particular applications, let alone deployments. However, if there is a direct path to any negative applications, the authors should point it out. For example, it is legitimate to point out that an improvement in the quality of generative models could be used to generate deepfakes for disinformation. On the other hand, it is not needed to point out that a generic algorithm for optimizing neural networks could enable people to train models that generate Deepfakes faster.
- The authors should consider possible harms that could arise when the technology is being used as intended and functioning correctly, harms that could arise when the technology is being used as intended but gives incorrect results, and harms following from (intentional or unintentional) misuse of the technology.
- If there are negative societal impacts, the authors could also discuss possible mitigation strategies (e.g., gated release of models, providing defenses in addition to attacks, mechanisms for monitoring misuse, mechanisms to monitor how a system learns from feedback over time, improving the efficiency and accessibility of ML).

## 11. Safeguards

Question: Does the paper describe safeguards that have been put in place for responsible release of data or models that have a high risk for misuse (e.g., pretrained language models, image generators, or scraped datasets)?

Answer: [\[NA\]](#)

Justification: We only release pretrained models on the benchmarks we evaluated our method, and do not believe these to pose such risks.

Guidelines:

- The answer NA means that the paper poses no such risks.
- Released models that have a high risk for misuse or dual-use should be released with necessary safeguards to allow for controlled use of the model, for example by requiring that users adhere to usage guidelines or restrictions to access the model or implementing safety filters.
- Datasets that have been scraped from the Internet could pose safety risks. The authors should describe how they avoided releasing unsafe images.
- We recognize that providing effective safeguards is challenging, and many papers do not require this, but we encourage authors to take this into account and make a best faith effort.

## 12. Licenses for existing assets

Question: Are the creators or original owners of assets (e.g., code, data, models), used in the paper, properly credited and are the license and terms of use explicitly mentioned and properly respected?

Answer: [\[Yes\]](#)

Justification: We've made our best effort to include all relevant citations and licenses in our paper and codebase.

Guidelines:

- The answer NA means that the paper does not use existing assets.
- The authors should cite the original paper that produced the code package or dataset.
- The authors should state which version of the asset is used and, if possible, include a URL.
- The name of the license (e.g., CC-BY 4.0) should be included for each asset.
- For scraped data from a particular source (e.g., website), the copyright and terms of service of that source should be provided.
- If assets are released, the license, copyright information, and terms of use in the package should be provided. For popular datasets, [paperswithcode.com/datasets](http://paperswithcode.com/datasets) has curated licenses for some datasets. Their licensing guide can help determine the license of a dataset.
- For existing datasets that are re-packaged, both the original license and the license of the derived asset (if it has changed) should be provided.
- If this information is not available online, the authors are encouraged to reach out to the asset's creators.

### 13. New assets

Question: Are new assets introduced in the paper well documented and is the documentation provided alongside the assets?

Answer: [NA]

Justification: We will provide detailed documentation alongside our codebase.

Guidelines:

- The answer NA means that the paper does not release new assets.
- Researchers should communicate the details of the dataset/code/model as part of their submissions via structured templates. This includes details about training, license, limitations, etc.
- The paper should discuss whether and how consent was obtained from people whose asset is used.
- At submission time, remember to anonymize your assets (if applicable). You can either create an anonymized URL or include an anonymized zip file.

### 14. Crowdsourcing and research with human subjects

Question: For crowdsourcing experiments and research with human subjects, does the paper include the full text of instructions given to participants and screenshots, if applicable, as well as details about compensation (if any)?

Answer: [NA]

Justification: Our paper does not involve crowdsourcing nor research with human subjects.

Guidelines:

- The answer NA means that the paper does not involve crowdsourcing nor research with human subjects.
- Including this information in the supplemental material is fine, but if the main contribution of the paper involves human subjects, then as much detail as possible should be included in the main paper.
- According to the NeurIPS Code of Ethics, workers involved in data collection, curation, or other labor should be paid at least the minimum wage in the country of the data collector.

### 15. Institutional review board (IRB) approvals or equivalent for research with human subjects

Question: Does the paper describe potential risks incurred by study participants, whether such risks were disclosed to the subjects, and whether Institutional Review Board (IRB) approvals (or an equivalent approval/review based on the requirements of your country or institution) were obtained?

Answer: [NA]

Justification: Our paper does not involve crowdsourcing nor research with human subjects.

Guidelines:

- The answer NA means that the paper does not involve crowdsourcing nor research with human subjects.
- Depending on the country in which research is conducted, IRB approval (or equivalent) may be required for any human subjects research. If you obtained IRB approval, you should clearly state this in the paper.
- We recognize that the procedures for this may vary significantly between institutions and locations, and we expect authors to adhere to the NeurIPS Code of Ethics and the guidelines for their institution.
- For initial submissions, do not include any information that would break anonymity (if applicable), such as the institution conducting the review.

#### 16. Declaration of LLM usage

Question: Does the paper describe the usage of LLMs if it is an important, original, or non-standard component of the core methods in this research? Note that if the LLM is used only for writing, editing, or formatting purposes and does not impact the core methodology, scientific rigorousness, or originality of the research, declaration is not required.

Answer: [NA]

Justification: LLMs are not important, original, or non-standard component of this research.

Guidelines:

- The answer NA means that the core method development in this research does not involve LLMs as any important, original, or non-standard components.
- Please refer to our LLM policy (<https://neurips.cc/Conferences/2025/LLM>) for what should or should not be described.